LETTER

https://doi.org/10.1038/s41586-018-0178-z

Disruption of *TET2* promotes the therapeutic efficacy of CD19–targeted T cells

Joseph A. Fraietta[1,2,3,4], Christopher L. Nobles[5], Morgan A. Sammons[6,10], Stefan Lundh[1,2], Shannon A. Carty[2,11], Tyler J. Reich[1,2], Alexandria P. Cogdill[1,2], Jennifer J. D. Morrissette[3], Jamie E. DeNizio[7,8], Shantan Reddy[5], Young Hwang[5], Mercy Gohil[1,2], Irina Kulikovskaya[1,2], Farzana Nazimuddin[1,2], Minnal Gupta[1,2], Fang Chen[1,2], John K. Everett[5], Katherine A. Alexander[6], Enrique Lin-Shiao[6], Marvin H. Gee[9], Xiaojun Liu[1,2], Regina M. Young[1,2], David Ambrose[1,2], Yan Wang[1,2], Jun Xu[1,2], Martha S. Jordan[2,3], Katherine T. Marcucci[1,2], Bruce L. Levine[1,2,3], K. Christopher Garcia[9], Yangbing Zhao[1,2], Michael Kalos[1,2,3], David L. Porter[1,2,7], Rahul M. Kohli[5,7,8], Simon F. Lacey[1,2,3], Shelley L. Berger[6], Frederic D. Bushman[5], Carl H. June[1,2,3,4]* & J. Joseph Melenhorst[1,2,3,4]*

Cancer immunotherapy based on genetically redirecting T cells has been used successfully to treat B cell malignancies[1–3]. In this strategy, the T cell genome is modified by integration of viral vectors or transposons encoding chimaeric antigen receptors (CARs) that direct tumour cell killing. However, this approach is often limited by the extent of expansion and persistence of CAR T cells[4,5]. Here we report mechanistic insights from studies of a patient with chronic lymphocytic leukaemia treated with CAR T cells targeting the CD19 protein. Following infusion of CAR T cells, anti-tumour activity was evident in the peripheral blood, lymph nodes and bone marrow; this activity was accompanied by complete remission. Unexpectedly, at the peak of the response, 94% of CAR T cells originated from a single clone in which lentiviral vector-mediated insertion of the CAR transgene disrupted the methylcytosine dioxygenase *TET2* gene. Further analysis revealed a hypomorphic mutation in this patient's second *TET2* allele. *TET2*-disrupted CAR T cells exhibited an epigenetic profile consistent with altered T cell differentiation and, at the peak of expansion, displayed a central memory phenotype. Experimental knockdown of *TET2* recapitulated the potency-enhancing effect of *TET2* dysfunction in this patient's CAR T cells. These findings suggest that the progeny of a single CAR T cell induced leukaemia remission and that TET2 modification may be useful for improving immunotherapies.

Here we describe an unusual case in which CAR T cell therapy was used to treat chronic lymphocytic leukaemia (CLL) that sheds light on the determinants of CAR-T cell efficacy and persistence. A seventy-eight-year-old man with advanced relapsed/refractory CLL (Patient-10, Supplementary Table 1) enrolled in a clinical trial for CD19 CAR T cell (CTL019) therapy (trial no. NCT01029366). He underwent two adoptive transfers of autologous CTL019 cells, approximately two months apart. Following the first infusion, he became persistently febrile and was diagnosed with cytokine release syndrome (CRS). Signs of CRS rapidly resolved following administration of interleukin (IL)-6 receptor-blocking therapy. Patient-10 continued to show progressive leukaemia six weeks after receiving his first dose of CAR T cells (Fig. 1a–c).

Because there was a concern that early blockade of IL-6-mediated signalling may have diminished the response to CAR T cell therapy, this patient was retreated with the remainder of his CAR T cells 70 days after the first dose (Supplementary Table 1). Infusions were again complicated by CRS, but this resolved without anti-IL-6 receptor-blocking intervention. Evaluation of the patient's bone marrow one month later revealed extensive infiltration of CLL (Extended Data Fig. 1), and computed tomography (CT) scans showed minimal improvement in extensive adenopathy. Unexpectedly, two months after the second infusion, the expansion of CAR T cells peaked in the peripheral blood, followed by contraction (Fig. 1a). CTL019 cell outgrowth occurred mostly in the $CD8^+$ T cell compartment, which is typical in patients with CLL who respond to CAR T cell treatment (Extended Data Fig. 2a). Delayed CAR T cell expansion was accompanied by high-grade CRS and elevated circulating levels of interferon (IFN)-γ, granulocyte-colony stimulating factor (G-CSF), IL-6, IL-8 and IL-10 (Fig. 1b). Coincident with the onset of high fever, rapid clearance of CLL was observed (Fig. 1c, d). Next-generation sequencing of rearrangement products at the immunoglobulin heavy chain (IGH) locus showed a 1-log reduction in tumour burden 51 days after the second infusion, with complete eradication of this tumour clone from the blood one month later (Supplementary Table 2). CT scans showed a marked improvement in mediastinal and axillary adenopathy (69% change; Fig. 1d). Patient-10 achieved a complete response with no evidence of CLL in his marrow (Extended Data Fig. 1, Supplementary Table 2) and resolution of all abnormal adenopathy six months later (Fig. 1d and data not shown). His most recent long-term follow-up evaluation (after more than 4.2 years) revealed the presence of CAR T cells in the peripheral blood, ongoing B cell aplasia (Extended Data Fig. 2b–e) and no evidence of circulating disease or marrow infiltration (Extended Data Fig. 1). Immune cell populations in the blood were normal in frequency, with no observed signs of lymphoproliferative abnormalities (Extended Data Fig. 2f and data not shown). The patient remains well in complete remission that has been sustained for more than five years at the time of this report.

Deep sequencing of the T cell receptor beta repertoire indicated that pre-infusion $CD8^+$ CTL019 cells and the peripheral blood CD8 T cell compartment one month after the second infusion were polyclonal, with multiple distinct TCRVβ clonotypes that were similar between the samples (Fig. 2a, Extended Data Fig. 3a). Approximately two months after the second infusion, TCRVβ5.1 family usage exhibited a skewing of greater than 50%, with clonal dominance occurring in $CD8^+$ CTL019 cells (Fig. 2a, b). Subsequent analysis revealed that 94% of the $CD8^+$ CAR T cell repertoire consisted of a single clone that was not detected at the time of transfer or one month after the second infusion (Fig. 2c). The expansion of this clonal population of cells declined in

[1]Center for Cellular Immunotherapies, Perelman School of Medicine, University of Pennsylvania, Philadelphia, PA, USA. [2]Abramson Cancer Center, Perelman School of Medicine, University of Pennsylvania, Philadelphia, PA, USA. [3]Pathology and Laboratory Medicine, Perelman School of Medicine, University of Pennsylvania, Philadelphia, PA, USA. [4]Parker Institute for Cancer Immunotherapy, University of Pennsylvania, Philadelphia, PA, USA. [5]Department of Microbiology, Perelman School of Medicine, University of Pennsylvania, Philadelphia, PA, USA. [6]Department of Cell and Developmental Biology, Epigenetics Program, Perelman School of Medicine, University of Pennsylvania, Philadelphia, PA, USA. [7]Department of Medicine, Perelman School of Medicine, University of Pennsylvania, Philadelphia, PA, USA. [8]Department of Biochemistry and Biophysics, Perelman School of Medicine, University of Pennsylvania, Philadelphia, PA, USA. [9]Department of Molecular and Cellular Physiology, Stanford University School of Medicine, Stanford, CA, USA. [10]Present address: Department of Biology, University at Albany, State University of New York, Albany, NY, USA. [11]Present address: Department of Internal Medicine and Rogel Cancer Center, University of Michigan, Ann Arbor, MI, USA. *e-mail: cjune@upenn.edu; mej@upenn.edu

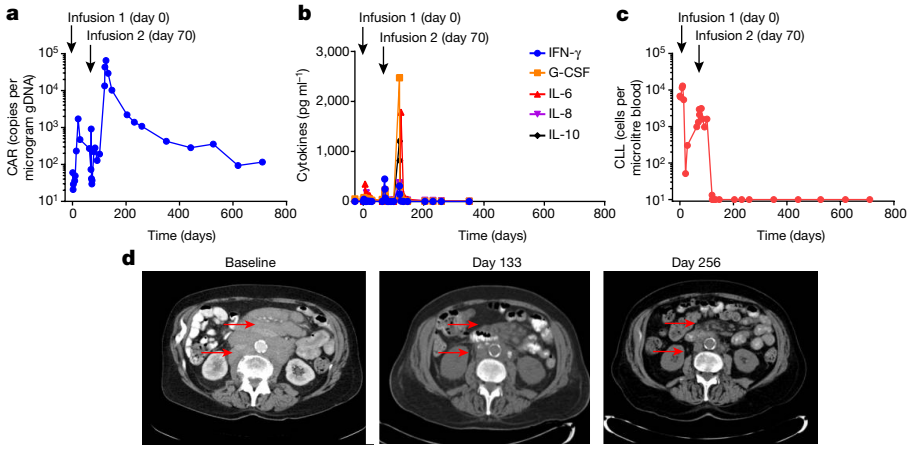

Fig. 1 | Evaluation of clinical responses following adoptive transfer of CAR T cells in a patient with CLL. a, In vivo expansion and persistence of CAR T cells. **b**, Longitudinal measurements of serum cytokines before and after CAR T cell infusions. **c**, Total number of circulating B-CLL cells before and after CTL019 therapy. **d**, Sequential CT imaging of chemotherapy-refractory lymphadenopathy. Red arrows indicate masses that were progressively reduced following the second CAR T cell infusion.

line with CAR T cell decay kinetics (Fig. 2d). Thus, leukaemia was eliminated in this patient primarily by the progeny of a single CAR T cell that demonstrated massive in vivo expansion (approximately 29 population doublings in the peripheral blood).

Longitudinal analysis of blood samples from Patient-10 revealed a highly abundant cell clone with an integration site in intron 9 of *TET2*, which was expanded in CAR T cells at the peak of clinical activity and not at earlier time points (Fig. 3a). This large degree of T cell clonal dominance has not been observed in more than forty leukaemia patients treated with CD19-directed T cells at the University of Pennsylvania, as determined by lentiviral integration site analysis (Extended Data Fig. 3b–d and data not shown). In CLL and acute lymphblastic leukaemia (ALL), accumulation of CAR T cells in vivo results from the expansion of a diverse polyclonal or pauciclonal repertoire within the transduced T cell population[6]. In Patient-10, cells bearing the *TET2* integration event were present in the blood at a relative abundance of 14% at 4.2 years after the infusion (Fig. 3a). The clonal population thus contracted, with no signs of insertional oncogenesis. Because *TET2* is a tumour suppressor gene, we are continuing to monitor this patient carefully.

TET2 is a master regulator of blood cell formation. Haploinsuffciency or deletion of *TET2* is found in normal clonal haematopoiesis[7] as well as the initiation of lymphoma and leukaemia, including naturally arising and human T-lymphotropic virus type 1 (HTLV-1)-associated malignancies[8–11]. Although *TET2* inactivation may contribute to increased self-renewal of haematopoietic stem and progenitor cells, its

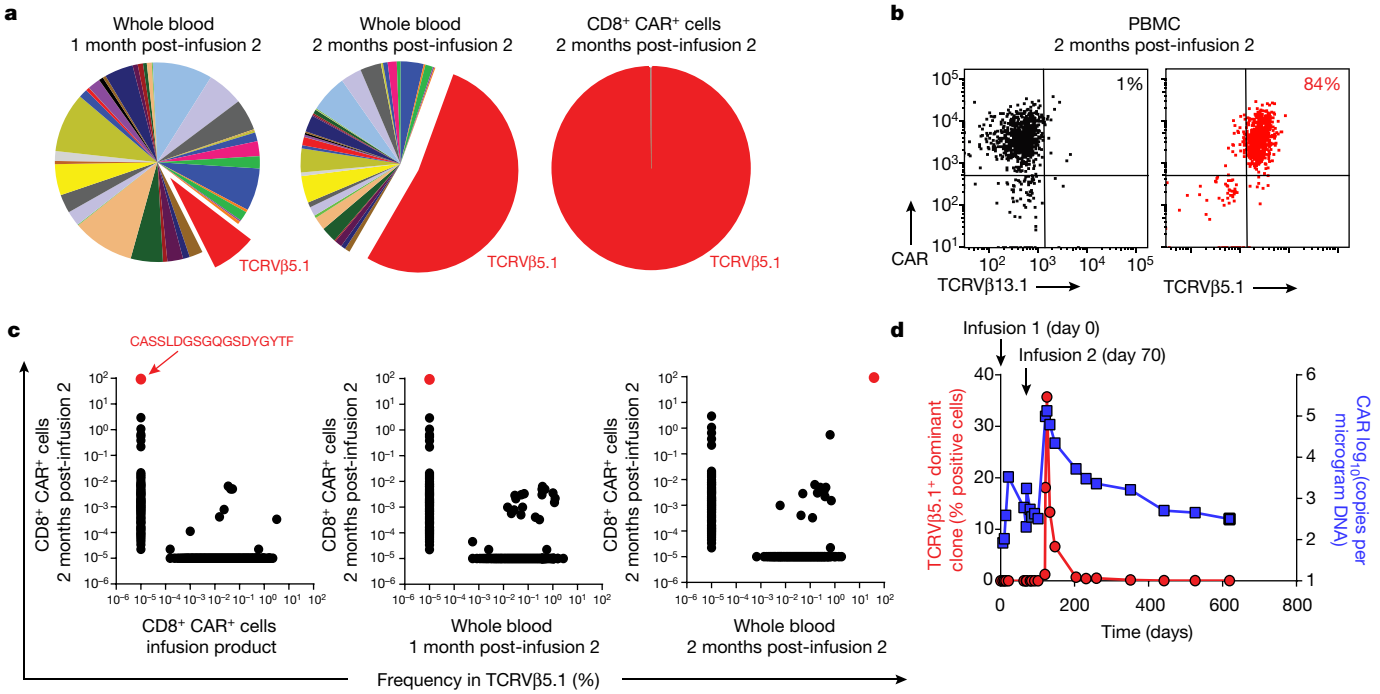

Fig. 2 | Analysis of CAR T cell clonal expansion in a patient with CLL who had a delayed therapeutic response. a, Frequency of TCRVβ gene segment usage in the blood of Patient-10 one month (left) and two months (middle) after the second CAR T cell infusion. TCRVβ clonotype frequencies in sorted CAR T cells at the peak of expansion are also shown (right). **b**, Flow cytometric proportions of TCRVβ5.1- versus TCRVβ13.1-positive (negative control) CAR T cells. **c**, Abundance of different TCRVβ5.1 clones in CAR$^+$ T cells at the peak of activity relative to other time points. Red dots indicate the dominant TCRVβ5.1 clone (representative of two independent experiments). **d**, Expansion kinetics of the TCRVβ5.1$^+$ dominant clone following a second infusion of CAR T cells plotted in parallel with CTL019 levels. Percentages of positive cells were calculated from the results of a quantitative PCR assay designed to amplify clonotype-specific sequences.

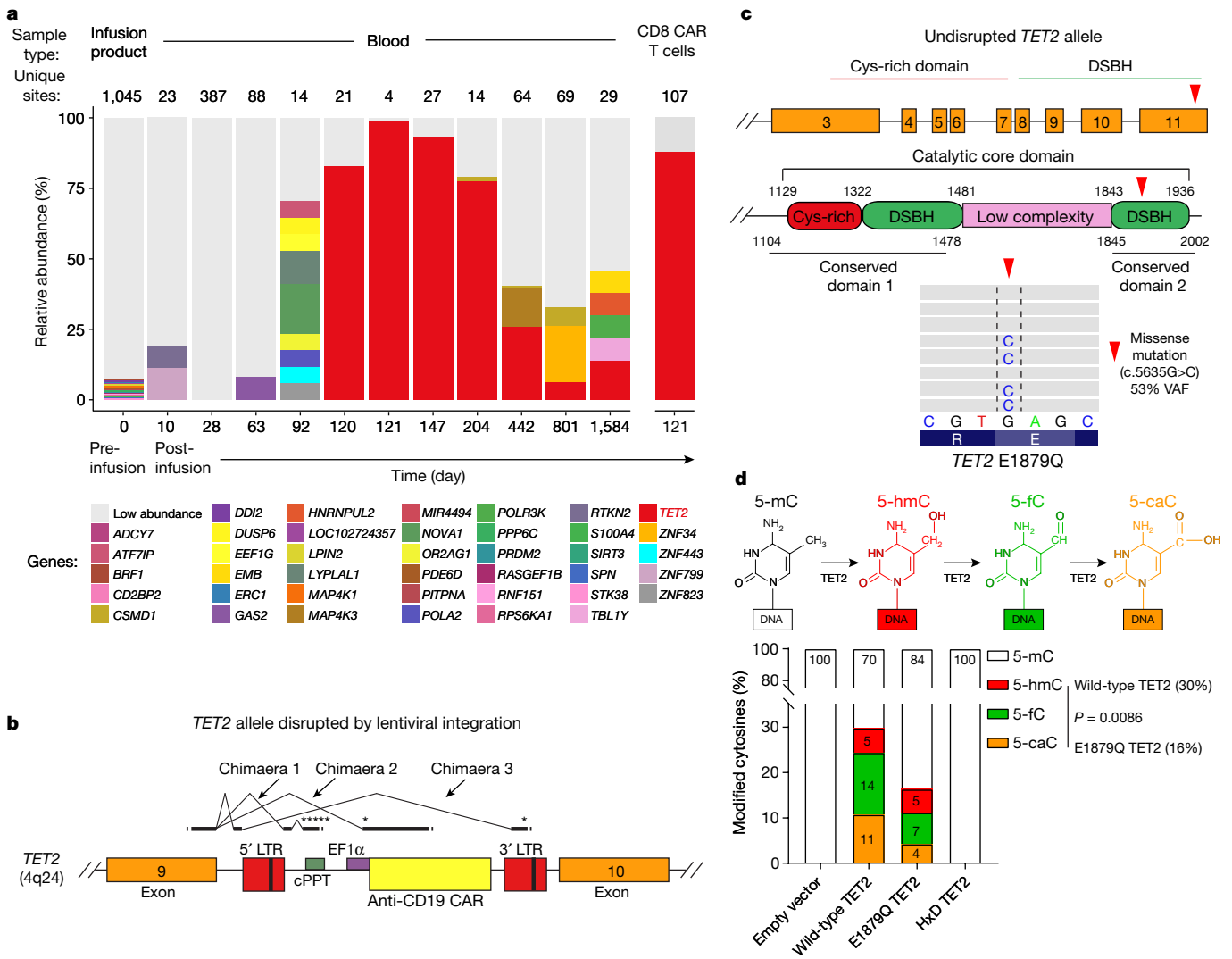

Fig. 3 | Investigation of CAR lentiviral integration sites and *TET2* dysfunction in Patient-10. a, Longitudinal CAR T cell clonal abundance as marked by integration sites. Different colours (horizontal bars) indicate major cell clones. A key to the sites, named for the nearest gene, is shown below the graph (abundances below 3% binned as 'Low abundance'). **b**, Diagram of the vector at the *TET2* integration site locus illustrating splicing into the vector provirus to yield truncated transcripts. Asterisks denote ectopic stop codons. LTR, long terminal repeat; cPPT, polypurine tract; EF1α, elongation factor 1-α promoter. **c**, Domain organization of TET2 and location of a residue mutated in CAR^+ and CAR^- T cells from Patient-10. Cysteine (Cys)-rich and catalytic double-stranded β-helix (DSBH) domains are also shown (red arrow denotes an amino acid change resulting from a missense mutation). Representative results of next generation sequencing appear beneath the structural diagrams. Each grey bar denotes a DNA fragment. A single-base G/C nucleotide substitution is highlighted by dashed lines above the consensus sequence. **d**, Diagram of the TET2-catalysed sequential oxidations of 5-mC to 5-hmC and to 5-fC and 5-caC (top). Genomic levels of 5-mC, 5-hmC, 5-fC, and 5-caC modifications produced by the E1879Q TET2 mutant shown as per cent of total cytosine modifications. Percentages derived from the mean of three independent experiments are shown. *P* values were determined using a two-tailed, paired Student's *t*-test.

disruption alone infrequently leads to overt oncogenesis[10,12]. Analysis of polyadenylated *TET2* RNA populations in clonal CAR T cells at the peak of expansion in Patient-10 showed the appearance of new chimaeric RNAs that spliced from *TET2* exon 9 into the vector and terminated, truncating the encoded protein with premature stop codons (Fig. 3b, Extended Data Fig. 4a, b). Although it is possible that expression of the truncated fusion TET2 protein may have a dominant-negative effect, it has been demonstrated that other TET2 mutant proteins do not exhibit such characteristics[13].

We next sequenced CAR^+ and CAR^- T cells from this subject and examined genes involved in haematologic malignancies (Extended Data Fig. 4c). In both samples, a missense variant in *TET2* encoding amino acid 1879 was found in the catalytic domain, converting the wild-type residue, glutamic acid, to glutamine (Fig. 3c and data not shown). The c.5635C mutation was present in the allele of *TET2* without the integrated CAR transgene, as that allele contained the wild-type reference sequence (c.5635G; Extended Data Fig. 4d). No other mutations were found in the panel of 67 additional genes analysed.

TET2 encodes methylcytosine dioxygenase, an enzyme that catalyses the conversion of 5-methylcytosine (5-mC) into 5-hydroxymethylcytosine (5-hmC) and the rarer bases 5-formylcytosine (5-fC) and 5-carboxylcytosine (5-caC), thereby mediating DNA demethylation[14–19] (Fig. 3d, top panel). Methylation at the C5 position of cytosine normally represses transcription, and therefore, demethylation is expected to activate gene expression. We interrogated the functional significance of the E1879Q mutation using plasmids encoding wild-type *TET2* or this *TET2* variant that were transfected into HEK293T cells (Extended Data Fig. 5a–c). Overexpression of wild-type or mutant TET2 proteins was verified by western blotting (Extended Data Fig. 5b, c). Analysis of genomic DNA isolated from these cells using both dot blotting (Extended Data Fig. 5a, b) and liquid chromatography–tandem mass spectrometry (LC–MS/MS) (Extended Data Fig. 5d, e) revealed that E1879Q compromises the step-wise

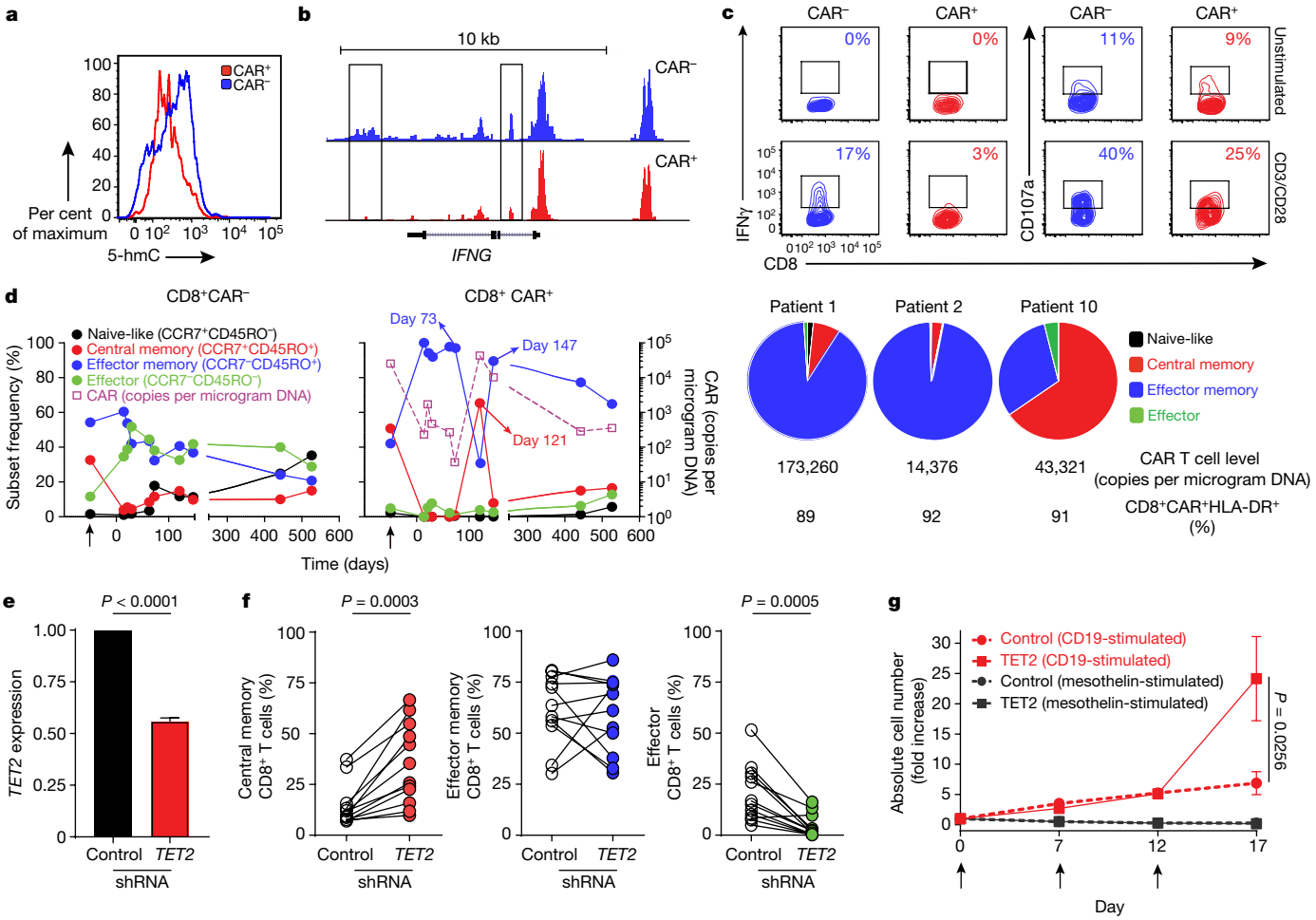

Fig. 4 | Effect of *TET2* alteration on the epigenetic landscape of CAR T cells. a, Total 5-hmC levels in CAR$^+$ and CAR$^-$ T cells cultured from Patient-10. Histograms depict the intensity of intracellular 5-hmC staining. **b**, Genome browser views of ATAC enrichment at the *IFNG* locus of T cells from Patient-10. **c**, Frequencies of IFNγ- and CD107a-expressing T cells expanded from Patient-10, unstimulated or stimulated with anti-CD3/CD28 antibodies. Insets indicate frequencies of gated cell populations. **d**, Longitudinal differentiation phenotypes of CAR$^-$ (left) and CAR$^+$ (middle) CD8$^+$ T cells from Patient-10. Black arrows denote pre-infusion CAR T cells. Differentiation phenotype at the peak of in vivo activity is shown in two patients with CLL who showed long-term complete responses (Patient-1 and Patient-2) compared to Patient-10 (right). Pie slices represent T cell subset frequencies. The CTL019 cell level and frequencies of activated CAR T cells expressing HLA-DR (surface molecule indicative of T cell activation) at the peak of each patient's response are listed below the pie charts. **e**, *TET2* expression in healthy donor CD8$^+$ T cells transduced with a scrambled shRNA (control) or *TET2* shRNA. Error bars depict s.e.m. **f**, Frequencies of central memory (left), effector memory (middle) and effector (right) CD8$^+$ T cells following shRNA-mediated knockdown of *TET2* ($n = 12$; pooled results from 4 independent experiments). **g**, Proliferation of healthy donor CTL019 cells ($n = 8$; 3 independent experiments) in response to repetitive stimulation (denoted by black arrows) with K562 cells expressing CD19 or mesothelin (negative control). CAR T cells were transduced to express either a scrambled control or *TET2*-specific shRNA. *P* values were determined using a two-tailed, paired Student's *t*-test. All error bars depict s.e.m.

oxidation of 5-mC relative to wild-type TET2, with reductions in 5-fC and 5-caC occurring (Fig. 3d). Therefore, the clonal expansion of CAR T cells in Patient-10 was comprised of a compound heterozygous loss-of-function in *TET2* on one allele and a hypomorphic E1879Q variant on the other allele.

CAR$^+$Vβ5.1$^+$ T cells from Patient-10 exhibited lower total levels of 5-hmC compared to their CAR$^-$Vβ5.1$^-$ T cell counterparts (Fig. 4a). This was presumably the result of disruption of the wild-type *TET2* allele following lentiviral integration, as the TET2 E1879Q variant can form 5-hmC (Fig. 3d, Extended Data Fig. 5a, b). To investigate the effects of *TET2* alteration on CAR T cell fate and function, we performed assay for transposase-accessible chromatin using sequencing (ATAC–seq), which monitors DNA accessibility (Supplementary Table 3). The global epigenetic changes between CAR$^+$ and CAR$^-$ T cells from Patient-10 were modest (Extended Data Fig. 6a). However, we found that genes with more accessible chromatin in CAR$^+$ compared to CAR$^-$ T cells were enriched in pathways that regulate the cell cycle and T cell receptor signalling (Extended Data Fig. 6b, Supplementary Tables 4, 5a). ATAC–seq peaks that were reduced or lost in the setting of *TET2* biallelic dysfunction included those corresponding to several regulators of T cell effector differentiation or exhaustion such as *IFNG*, *NOTCH2*, *CD28*, *ICOS* and *PRDM1* (Fig. 4b, Extended Data Fig. 6c, Supplementary Tables 4, 5b). Furthermore, transcription factor motifs within sites that changed accessibility could have affected specific transcriptional circuits controlling CAR T cell fate and anti-tumour activity in this patient (Extended Data Fig. 6d, Supplementary Table 6a, b). Functional analysis of CAR$^+$ T cells with biallelically altered *TET2* cultured from this patient showed a diminished capacity to express IFNγ and CD107a (a degranulation marker) when activated (Fig. 4c), consistent with a less differentiated state. Thus, lentiviral integration into *TET2* together with a hypomorphic mutation on the second allele reprogrammed the epigenetic landscape of CAR T cells in a manner that was consistent with altered T lymphocyte differentiation.

We next analysed the differentiation state of ex vivo CTL019 cells from Patient-10 and compared it to those of CAR T cells from six other patients who responded to this therapy (Extended Data Fig. 7), including two subjects with CLL (Patient-1 and Patient-2) who had long-term durable remissions (of more than 6 years) and did not have

TET2 integrations (data not shown). At the peak of in vivo expansion and activation marker expression, 65% of the CAR T cells in Patient-10 had a central memory phenotype (Fig. 4d, Extended Data Fig. 7a) which differed from other responders whose repertoires were dominated by $CD8^+$ effector memory and effector CTL019 cells at the height of the response (Fig. 4d, Extended Data Fig. 7b). Experimental knockdown of *TET2* (Fig. 4e) recapitulated the effect of its dysfunction in Patient-10 on the differentiation state of both total and CAR^+CD8^+ as well as $CD4^+$ primary T cells (Fig. 4f, Extended Data Fig. 8a, b), implicating TET2 as an epigenetic modulator of human T lymphocyte fate. TET2-mediated regulation of $CD8^+$ T cell differentiation may not occur at the transcriptional level, as we did not observe differential *TET2* mRNA expression between naive and memory subsets (Extended Data Fig. 8c).

To investigate the effects of TET2 inhibition on CAR T cell function, we performed an in vitro serial re-stimulation assay. Repeated stimulation with CD19-expressing tumour cells enabled *TET2* knockdown CAR T cells to continue to expand in an antigen-dependent manner, whereas re-stimulation of CAR T cells with unaltered TET2 resulted in arrest of culture growth (Fig. 4g) without affecting viability (Extended Data Fig. 8d). We next examined cytokine production following acute (Extended Data Fig. 9a) and chronic (Extended Data Fig. 9b, c) antigen stimulation. Consistent with our analysis of $CD8^+CAR^+$ T cells in Patient-10, IFNγ production following activation of CD3 and CD28 was diminished in $CD8^+$ as well as $CD4^+$ T cells with reduced TET2 levels (Extended Data Fig. 9a). A similar decrease was observed for TNFα generation (Extended Data Fig. 9a). By contrast, acute production of both TNFα and IL-2 by $CD4^+$ T cells was increased upon CAR-specific stimulation (Extended Data Fig. 9a). While repeated exposure of bulk CTL019 cells to CD19-expressing tumours also led to decreased IFNγ elaboration (Extended Data Fig. 9b, c), TET2 inhibition resulted in the sustained production of various other cytokines following multiple rounds of stimulation (Extended Data Fig. 9b). Thus, *TET2* may control human T cell subset-specific cytokine production in an antigen-receptor-dependent and/or co-stimulatory signal-dependent fashion.

On the basis of our evaluation of CAR^+ T cells expanded from Patient-10, we predicted that knockdown of *TET2* would decrease effector molecule expression. Unexpectedly, CAR-specific stimulation, but not CD3 and CD28 stimulation, increased the expression of CD107a (Extended Data Fig. 10a). This may be attributed, at least in part, to enhanced cytolytic capacity mediated by 4-1BB over CD28 co-stimulation due to NKG2D upregulation[20]. Because $CD8^+$ T cell differentiation is accompanied by decreased methylation and upregulated gene expression at effector gene loci, including *GZMB* (encoding granzyme B) and *IFNG*[21], we subsequently investigated whether TET2 inhibition influences critical components of the cytotoxic machinery. In contrast to IFNγ, TET2 reduction in $CD8^+$ CAR^+ T cells increased granzyme B and perforin expression (Extended Data Fig. 10b). These changes were associated with the heightened cytotoxic activity of *TET2* knockdown CAR T cells (Extended Data Fig. 10c).

The above findings suggest that TET2 dysfunction may produce potent CAR T cells with properties of short-lived memory cells that can expand and elicit effector responses, as well as long-lived, persistent memory cells. We thus examined additional effector or memory markers in $CD8^+CAR^+$ and CAR^- T cells using post-infusion samples from Patient-10 and other long-term responding patients with CLL. At the height of the response, tumour-reactive CAR^+ T cells from Patient-10 possessed higher levels of granzyme B (Extended Data Fig. 11a) and eomesodermin (Eomes; a transcription factor involved in the formation and maintenance of the $CD8^+$ memory T cell pool; Extended Data Fig. 11b) compared to matched CAR^- T cells, unlike the other complete responders. All clinically active $CD8^+$ CAR^+ T cells in these patients expressed CD27, a co-stimulatory receptor involved in the generation of T cell memory (Extended Data Fig. 11b). The frequency of CTL019 cells expressing KLRG1, a marker of T lymphocyte senescence that is known to be regulated by DNA methylation[21], was significantly lower on CAR^+ T cells from Patient-10 than on cells from other patients (Extended Data Fig. 11b). A high frequency of Ki-67-positive CAR^+ T cells was observed at the peak of in vivo expansion in Patient-10 (Extended Data Fig. 11a), further suggesting that TET2 is required for CAR-specific $CD8^+$ T cell proliferation. These observations collectively support the idea that TET2 dysfunction promotes the development of human memory CAR T cells that can elicit effective anti-tumour responses. The remission observed in Patient-10 was likely to result from the marked increase in the number of CTL019 cells with TET2 dysfunction, despite the reduction in certain effector functions.

In summary, profound clonal expansion of a single CAR-transduced T cell with biallelic *TET2* dysfunction transformed a non-curative response into a deep molecular remission in a seventy-eight-year-old patient with CLL. Characterization of this T lymphocyte population revealed that changes to the epigenetic environment altered the differentiation state and proliferative capacity of the cells and translated into a considerable therapeutic effect. Although our initial studies were based on an extensive analysis of one subject, recapitulation of the effect of *TET2* dysfunction on CAR T cell fate and anti-tumour activity in relevant culture systems involving primary human T-lymphocytes supports the discovery of a modifiable epigenetic pathway that can shape the immune response. Thus, targeting the epigenome may improve the efficacy and persistence of CAR T cells. Finally, our results indicate that the progeny of a single CAR T cell are sufficient to mediate potent anti-tumour effects in advanced leukaemia, a finding that has substantial clinical implications regarding the delivery of bespoke cellular therapies.

Online content

Any Methods, including any statements of data availability and Nature Research reporting summaries, along with any additional references and Source Data files, are available in the online version of the paper at https://doi.org/10.1038/s41586-018-0178-z.

Received: 19 February 2017; Accepted: 27 April 2018;
Published online 30 May 2018.

1. Porter, D. L., Levine, B. L., Kalos, M., Bagg, A. & June, C. H. Chimeric antigen receptor-modified T cells in chronic lymphoid leukemia. *N. Engl. J. Med.* **365**, 725–733 (2011).
2. Schuster, S. J. et al. Chimeric antigen receptor T cells in refractory B cell lymphomas. *N. Engl. J. Med.* **377**, 2545–2554 (2017).
3. Maude, S. L. et al. Tisagenlecleucel in children and young adults with B cell lymphoblastic leukemia. *N. Engl. J. Med.* **378**, 439–448 (2018).
4. Porter, D. L. et al. Chimeric antigen receptor T cells persist and induce sustained remissions in relapsed refractory chronic lymphocytic leukemia. *Sci. Transl. Med.* **7**, 303ra139 (2015).
5. Savoldo, B. et al. CD28 costimulation improves expansion and persistence of chimeric antigen receptor-modified T cells in lymphoma patients. *J. Clin. Invest.* **121**, 1822–1826 (2011).
6. Turtle, C. J. et al. CD19 CAR-T cells of defined $CD4^+$:$CD8^+$ composition in adult B cell ALL patients. *J. Clin. Invest.* **126**, 2123–2138 (2016).
7. Busque, L. et al. Recurrent somatic *TET2* mutations in normal elderly individuals with clonal hematopoiesis. *Nat. Genet.* **44**, 1179–1181 (2012).
8. Tefferi, A. et al. Detection of mutant TET2 in myeloid malignancies other than myeloproliferative neoplasms: CMML, MDS, MDS/MPN and AML. *Leukemia* **23**, 1343–1345 (2009).
9. Delhommeau, F. et al. Mutation in *TET2* in myeloid cancers. *N. Engl. J. Med.* **360**, 2289–2301 (2009).
10. Quivoron, C. et al. TET2 inactivation results in pleiotropic hematopoietic abnormalities in mouse and is a recurrent event during human lymphomagenesis. *Cancer Cell* **20**, 25–38 (2011).
11. Yeh, C. H. et al. Mutation of epigenetic regulators TET2 and MLL3 in patients with HTLV-I-induced acute adult T cell leukemia. *Mol. Cancer* **15**, 15 (2016).
12. Zang, S. et al. Mutations in 5-methylcytosine oxidase TET2 and RhoA cooperatively disrupt T cell homeostasis. *J. Clin. Invest.* **127**, 2998–3012 (2017).
13. Aslanyan, M. G. et al. Clinical and biological impact of TET2 mutations and expression in younger adult AML patients treated within the EORTC/GIMEMA AML-12 clinical trial. *Ann. Hematol.* **93**, 1401–1412 (2014).
14. Tahiliani, M. et al. Conversion of 5-methylcytosine to 5-hydroxymethylcytosine in mammalian DNA by MLL partner TET1. *Science* **324**, 930–935 (2009).
15. Kriaucionis, S. & Heintz, N. The nuclear DNA base 5-hydroxymethylcytosine is present in Purkinje neurons and the brain. *Science* **324**, 929–930 (2009).
16. Ito, S. et al. Role of Tet proteins in 5mC to 5hmC conversion, ES-cell self-renewal and inner cell mass specification. *Nature* **466**, 1129–1133 (2010).
17. Pfaffeneder, T. et al. The discovery of 5-formylcytosine in embryonic stem cell DNA. *Angew. Chem.* **50**, 7008–7012 (2011).

18. He, Y. F. et al. Tet-mediated formation of 5-carboxylcytosine and its excision by TDG in mammalian DNA. *Science* **333**, 1303–1307 (2011).
19. Ito, S. et al. Tet proteins can convert 5-methylcytosine to 5-formylcytosine and 5-carboxylcytosine. *Science* **333**, 1300–1303 (2011).
20. Zhang, H. et al. 4-1BB is superior to CD28 costimulation for generating CD8+ cytotoxic lymphocytes for adoptive immunotherapy. *J. Immunol.* **179**, 4910–4918 (2007).
21. Scharer, C. D., Barwick, B. G., Youngblood, B. A., Ahmed, R. & Boss, J. M. Global DNA methylation remodeling accompanies CD8 T cell effector function. *J. Immunol.* **191**, 3419–3429 (2013).

Acknowledgements L. Tian, V. Gonzalez, N. Kengle, J. Scholler, Y. Wu, A. Bagg, C. Pletcher, B. Carreno, A. Bigdeli and A. Chew are acknowledged for research support. D. Campana and C. Imai provided the CD19-directed CAR under material transfer agreements. B. Jena and L. Cooper provided the CAR anti-idiotypic antibody. The OSU-CLL cell line was a kind gift from J. C. Byrd. This work was supported by funding from NCI T32CA009140 (J.A.F.), P01CA214278 (C.H.J.), AI104400, AI 082020, AI045008, AI117950 (F.D.B), NIAID K08AI101008 (S.A.C.), NIGMS R01GM118501 (R.M.K.), R01CA165206 (D.L.P. and C.H.J.), a Stand Up to Cancer Phillip A. Sharp Innovation in Collaboration Award (S.L.B. and C.H.J.) and Novartis.

Reviewer information *Nature* thanks M. Maus and the other anonymous reviewer(s) for their contribution to the peer review of this work.

Author contributions J.A.F., C.L.N., M.A.S., S.A.C., J.J.D.M., R.M.Y., M.S.J., K.T.M., B.L.L., K.C.G., Y.Z., M.K., D.L.P., R.M.K., S.F.L., S.L.B., F.D.B, C.H.J. and J.J.M. designed experiments. J.A.F., C.L.N., M.A.S., S.L., S.A.C., T.R., A.P.C., J.J.D.M., J.E.D., S.R., Y.H., M.G., I.K., F.N., M.G., F.C., J.K.E., K.A.A., E.L.-S., M.H.G., X.L., D.A., Y.W. and J.X. performed experiments and/or analysed data. J.A.F., F.D.B., C.H.J. and J.J.M. wrote and edited the manuscript, with all authors providing feedback.

Competing interests J.A.F., C.L.N., R.M.Y., B.L.L., M.K., D.L.P., S.F.L., F.D.B., C.H.J. and J.J.M. hold patents related to CTL019 cell therapy. These authors declare no additional competing interests. The remaining authors declare no competing interests.

Additional information
Extended data is available for this paper at https://doi.org/10.1038/s41586-018-0178-z.
Supplementary information is available for this paper at https://doi.org/10.1038/s41586-018-0178-z.
Reprints and permissions information is available at http://www.nature.com/reprints.
Correspondence and requests for materials should be addressed to C.H.J. or J.J.M.
Publisher's note: Springer Nature remains neutral with regard to jurisdictional claims in published maps and institutional affiliations.

METHODS

Patient samples. Patients were enrolled in institutional review board (IRB)-approved clinical protocol: 'Genetically engineered lymphocyte therapy in treating patients with B cell leukemia or lymphoma that is resistant or refractory to chemotherapy' (ClinicalTrials.gov number: NCT01029366) which was designed to evaluate the safety and efficacy of the adoptive transfer of autologous T cells expressing CD19 chimaeric antigen receptors (CAR19) that incorporate TCR-ζ and 4-1BB costimulatory domains (CTL019). Participants provided written informed consent in accordance with the Declaration of Helsinki and the International Conference on Harmonization Guidelines for Good Clinical Practice. All regulations were followed according to this United States (US) Food and Drug Administration (FDA)-approved clinical protocol. The current study is a secondary investigation using patient samples collected from existing clinical trials. Therefore, the sample sizes in this report were determined by the original clinical trial designs and sample availability; no additional inclusion/exclusion criteria were applied.

Cell lines. NALM-6, K562 and HEK293T cell lines were originally obtained from the American Type Culture Collection (ATCC). OSU-CLL cells[22] were obtained from Ohio State University. Cells were expanded in RPMI medium containing 10% fetal bovine serum (FBS), penicillin and streptomycin at a low passage and tested for mycoplasma using the MycoAlert detection kit as per the manufacturer's (Lonza) instructions. Authentication of cell lines was performed by the University of Arizona (USA) Genetics Core based on criteria established by the International Cell Line Authentication Committee. Short tandem repeat (STR) profiling revealed that these cell lines were well above the 80% match threshold. NALM-6 and OSU-CLL cells were engineered to constitutively express click beetle green (CBG) luciferase/enhanced GFP (eGFP). K562 cells were transduced with a lentiviral vector encoding human CD19 (K562-CD19), and negative control cells were K562 cells expressing mesothelin (K562-mesothelin)[23]. Following transgene introduction, cells were sorted on a FACSAria (BD) to obtain a >99% pure population. Mycoplasma and authentication testing were routinely performed before and after molecular engineering.

CAR T cell manufacturing and correlative studies. Peripheral blood T cells for CTL019 cell manufacturing were obtained by leukapheresis as previously described[1,4]. The processing, flow cytometric evaluation, quantification of cytokines and quantitative PCR analyses (that is, detection of CAR19 and the TCRVβ5.1$^+$ dominant clone) on pre- and post-CTL019 infusion samples were conducted as previously reported[24]. Next-generation sequencing of immunoglobulin heavy chain (IGH) rearrangements was carried out on DNA isolated from blood and marrow samples. In brief, primers specific for the variable and joining gene segments of the third complementarity-determining region of the IGH were used for amplification and deep sequencing to identify the leukaemic clone relative to baseline samples (Adaptive Biotechnologies). The frequency of the leukaemic clone in each sample was calculated using the number of total and unique productive reads.

Population doublings of clonal CAR T cells in the blood (assuming a 5-litre volume of peripheral blood) were calculated using the equation $A_t = A_0 2^n$, in which n is the number of population doublings, A_0 is the input number of cells (assuming a single *TET2*-disrupted cell), and A_t is the number of CAR T cells at day 121 (peak CAR T cell expansion; 95.445 CD3$^+$ CD8$^+$ CAR$^+$ cells per microlitre whole blood).

These correlative assays were carried out at time points defined by the clinical protocol in parallel with disease response evaluations. This clinical trial was a single-treatment study; comparisons between patients in the current study were defined by the observed clinical responses. Investigators were blinded to clinical responses as correlative assays were conducted using de-identified subject samples.

Flow cytometry. Routine assessments of CAR T cell expansion and persistence as well as measurement of B-CLL burden in the blood and marrow were conducted according to our previously published methods using a six-parameter Accuri C6 flow cytometer (BD)[1,4]. T cell immunophenotyping was performed by surface staining with flow cytometry antibodies immediately following pre-incubation with Aqua Blue dead cell exclusion dye (Invitrogen). The Alexa Fluor 647–conjugated monoclonal antibody that was used to detect the CAR molecule has previously been described[25]. Commercially available flow cytometry antibodies against the following antigens used in the study are as follows: CD3 allophycocyanin (APC) H7, CCR7 PE/CF594, CD107a APC, (BD Biosciences); CD45RO brilliant violet (BV)570, CD8 BV650, CD4 BV785, perforin BV421, Ki-67 Alexa Fluor (AF)700, TNFα BV605 (Biolegend); TCRVβ5.1 APC, IFNγ PE, IL-2 PerCP-eFluor 710, Eomes FITC (eBioscience); Granzyme B PE/cyanine5.5 (Invitrogen). For intracellular staining, cells were fixed and permeabilized using the Foxp3 Fixation/Permeabilization Kit (eBioscience) or the Cytofix/Cytoperm Kit (BD Biosciences). The GolgiStop protein transport inhibitor containing monensin and GolgiPlug protein transport inhibitor containing brefeldin A (BD Biosciences) were used when staining for intracellular cytokine production. All flow cytometry reagents were titrated before use. Samples were acquired on an LSRFortessa (BD) and data were analysed using FlowJo software (TreeStar).

TCRVβ deep sequencing. Genomic DNA from pre-infusion T cells, peripheral blood samples or sorted post-infusion T cells was isolated using the DNeasy Blood and Tissue Kit (Qiagen). TCRVβ deep sequencing was carried out by immunoSEQ (Adaptive Biotechnologies). Only productive TCR rearrangements were used in the assessment of TCR clonotype frequencies.

Integration site analysis. Vector integration sites were detected from genomic DNA as described previously[26–29]. Genomic sequences were aligned to the human genome by BLAT (hg38, version 35, >95% identity) and statistical methods for analysing integration site distributions were carried out as previously described[30]. The SonicAbundance method was used to infer the abundance of cell clones from integration site data[28]. All samples were analysed independently in quadruplicate to suppress founder effects in the PCR and stochastics of sampling.

Detection of *TET2* chimaeric transcripts. RNA was isolated from cells and used as template with the One-Step RT–PCR Kit (Qiagen). Primers were designed to target the exon 9 and 10 boundaries of *TET2*, flanking the vector integration site and sequences internal to the anti-CD19BBζ CAR lentiviral vector. These included various regions of the vector sequence (Extended Data Fig. 4a). Reactions were carried out as per the manufacturer's specifications. Thermocycling temperatures and time for reverse transcription as well as PCR activation were conducted using the following cycling conditions: 30 s at 94 °C for melting, 30 s at 57 °C for primer annealing and 1.5 min at 72 °C for primer extension (35 cycles). A final extension at 72 °C was held for 10 min for each sample. PCR products were visualized on ethidium bromide agarose gels (1.5% by weight) via electrophoresis and ultraviolet imaging.

Next-generation sequencing of post-infusion CAR T cell samples. CAR$^+$ and CAR$^-$ CD8$^+$ T cells were purified from post-infusion PBMC samples corresponding to the peak of in vivo expansion in Patient-10. T cells were sorted using a FACSAria (BD) and genomic DNA was isolated from these lymphocytes as described above. A custom targeted next-generation sequencing panel of 68 genes associated with haematologic malignancies was then used (TruSeq Custom Amplicon, Illumina), and sequencing was carried out on an Illumina MiSeq (Illumina). A minimal mean depth of 2,110 reads was achieved for the specimens sequenced, with the assay and bioinformatics performed as previously described[31]. The data presented are based on human reference sequence UCSC build hg 19 (NCBI build 37.1).

Identifying the *TET2* allele hosting vector integration. A PCR assay was developed to amplify the region of DNA (approximately 4 kb) between the vector integration and the locus of the c.5635G>C mutation. Primers were designed to anneal to the vector sequence (MKL-3: 5′-CTTAAGCCTCAATAAAGCTTGCCTTGAG-3′) and multiple locations downstream of the mutation, chr4:105,276,145 (50 bp: 5′ GCTGGTAAAAGACGAGGGAGATCCTG-3′, 99 bp: 5′-GGCTT CCCAAAGAGCCAAGCCATG-3′, 120 bp: 5′-CACGGGCTTTTTCA GCCATTTTGGC-3′). Genomic DNA samples from sorted CAR$^+$ and CAR$^-$ CD8$^+$ T cells corresponding to the peak of clonal expansion in Patient-10 were selected for amplification. PCR reactions were carried out with Long Amp *Taq* polymerase (New England BioLabs) and 100–400 ng of DNA isolated from samples, according to the manufacturer's recommendations. Amplification was conducted as follows: 94 °C for 30 s, 30 cycles of (94 °C for 30 s, 60 °C for 30 s, and 65 °C for 3 min 20 s), and a final extension of 65 °C for 10 min. Amplified products were separated by electrophoresis on a 1% ethidium bromide agarose gel and prominent bands of 4 kb in size were isolated using the QIAquick Gel Extraction Kit (Qiagen). Isolated bands were ligated into pCR2.1 and cloned into TOP-10 chemically competent cells using the TOPO TA Cloning Kit (Invitrogen). Purified plasmids were sequenced with M13 forward and reverse primers using standard Sanger technology. Sequencing results were aligned to the vector sequence and reference genome.

Characterization of the TET2 E1879Q mutation. The previously characterized and crystalized human TET2-CS variant (1129–1936 Δ1481–1843) with an N-terminal FLAG-tag was expressed using a pLEXm expression vector[32,33]. The E1879Q mutation or mutation of the catalytic H1382Y and D1384A (HxD mutant) were generated by standard means. HEK293T cells were cultured in DMEM with GlutaMAX (Thermo Fisher Scientific) and 10% FBS (Sigma). Cells were transfected with wild-type (WT), mutant hTET2-CS or an empty pLEXm vector control using Lipofectamine 2000 (Thermo Fisher Scientific) according to the manufacturer's protocol. Medium was changed 24 h after transfection, and cells were collected by trypsinization 48 h after transfection and resuspended in phosphate-buffered saline. Genomic DNA was isolated from four-fifths of the cells using the DNeasy Blood and Tissue Kit (Qiagen) and the remaining one-fifth of the cells were lysed using CytoBuster Protein Extraction Reagent (EMD Millipore) for western blot analysis.

DNA blots for cytosine modifications were carried out according to established protocols[34]. Purified DNA from HEK293T cells was diluted to 15 ng/μl in Tris–EDTA (TE) buffer, pH 8.0 for twofold dilutions of each sample. One-quarter volume of 2 M NaOH–50 mM EDTA was added to each sample. The DNA was

denatured for 10 min at 95 °C and transferred quickly to ice, followed by the addition of 1:1 ice cold 2 M ammonium acetate. Polyvinylidene difluoride (PVDF) membranes were cut to size, wet with MeOH and equilibrated in TE buffer and then assembled into the PR 648 Slot Blot Manifold (GE Healthcare Life Sciences). Each well was washed with 400 µl TE drawn through with gentle vacuum, and genomic DNA was loaded, followed by another TE wash. Membranes were blocked for 2 h in 5% milk-TBST, washed thrice with TBST, and blotted at 4 °C overnight with primary antibodies against each modified cytosine (1:5,000 mouse anti-5-mC (Abcam); 1:10,000 rabbit anti-5-hmC (Active Motif); 1:5,000 rabbit anti-5-fC (Active Motif); 1:10,000 rabbit anti-5-caC (Active Motif)). Blots were then washed, incubated with a 1:2,000 dilution of a secondary horse anti-mouse-horseradish peroxidase (HRP; Cell Signaling Technology) or 1:5,000 goat anti-rabbit-HRP (Santa Cruz Biotechnology) for 2 h, washed and imaged using the Immobilon Western Chemiluminescent HRP Substrate (Millipore) and the Amersham Imager 600 (GE Healthcare Life Sciences).

For protein detection, clarified cell lysates were run on 8% sodium dodecyl sulphate polyacrylamide (SDS–PAGE) gels. Gels were transferred together onto a PVDF membrane using the iBlot 2 Gel Transfer Device (Thermo Fisher Scientific). Membranes were blocked for 2 h at room temperature with 5% (w/v) milk in Tris-buffered saline with 0.1% (v/v) Tween-20 (TBST), washed three times with TBST and blotted either with primary 1:10,000 anti-FLAG M2 (Sigma) or 1:1,000 anti-Hsp90α/β (Santa Cruz Biotechnology) antibodies at 4 °C overnight. Following incubation, membranes were washed and blotted with a 1:5,000 dilution of secondary goat anti-mouse-HRP antibodies (Santa Cruz Biotechnology) for 2 h, washed and imaged with Immobilon Western Chemiluminescent HRP Substrate (Millipore) on an Amersham Imager 600 (GE Healthcare Life Sciences).

For LC–MS/MS, 1–2 µg of genomic DNA from each sample was degraded to component nucleosides with 1 U DNA Degradase Plus (Zymo Research Corporation) at 37 °C overnight. The nucleoside mixture was diluted tenfold into 0.1% formic acid, and injected onto an Agilent 1200 Series HPLC with a 5 µm, 2.1 × 250 mm Supelcosil LC-18-S analytical column (Sigma) equilibrated to 45 °C in buffer A (5 mM ammonium formate, pH 4.0). The nucleosides were separated in a gradient of 0–15% buffer B (4 mM ammonium formate, pH 4.0, 20% (v/v) methanol) over 8 min at a flow rate of 0.5 ml per minute. Tandem MS was performed by positive ion mode ESI on a 6460 triple-quadrupole mass spectrometer (Agilent) with a gas temperature of 250 °C, a gas flow of 12 l/min, a nebulizer pressure of 35 psi, a sheath gas temperature of 300 °C, a sheath gas flow of 11 l/min, a capillary voltage of 3,500 V, a fragmentor voltage of 70 V and a delta EMV of +1,000 V. Collision energies were optimized to 10 V for 5-mC and 5-fC; 15 V for 5-caC; and 25 V for 5-hmC. Multiple reaction monitoring (MRM) mass transitions were 5-mC 242.11→126.066 *m/z*; 5-hmC 258.11→124.051; 5-fC 256.09→140.046; 5-caC 272.09→156.041; and T 243.10→127.050. Standard curves were generated using standard nucleosides (Berry & Associates) ranging from 2.5 µM to 610 pM (12.5 pmol to 3 fmol total). Digested oligonucleotides containing equimolar amounts of each modified cytosine were used as quality control samples. The sample peak areas were fit to the standard curve, as adjusted by the quality control samples to determine the amount of each modified cytosine in the genomic DNA sample. Amounts are expressed as the percentage of total cytosine modifications.

Measurement of total 5-hydroxymethylcytosine levels. $CD8^+$ T cells were purified from post-infusion PBMC samples using the EasySep Human $CD8^+$ T cell Immunomagnetic Negative Selection Kit (StemCell Technologies) and expanded ex vivo using a previously reported rapid expansion protocol[35]. Following culture, $CD8^+CAR^+TCRV\beta5.1^+$ and $CD8^+CAR^-TCRV\beta5.1^-$ T cells were sorted on a FACSAria (BD). Cells were permeabilized and treated with 300 µg/ml DNase I for 60 min at 37 °C. After washing, samples were incubated with an anti-5-hmC monoclonal antibody or an isotype control for 30 min, followed by staining with an Alexa Fluor 647-conjugated secondary antibody, as previously described[36]. Cells were immediately acquired on an LSRFortessa (BD).

Global chromatin profiling by ATAC–seq. Following culture, $CD8^+CAR^+TCRV\beta5.1^+$ and $CD8^+CAR^-TCRV\beta5.1^-$ T cells were sorted on a FACSAria (BD). ATAC–seq was carried out as previously described[37,38]. Two replicates were performed for each ex vivo expanded $CD8^+CAR^+TCRV\beta5.1^+$ and $CD8^+CAR^-TCRV\beta5.1^-$ T cell culture. In brief, nuclei were isolated from 200,000 sorted $CD8^+$ T cells for each replicate, followed by the transposition reaction in the presence of Tn5 transposase (Illumina) for 45 min at 37 °C. Purification of transposed DNA was subsequently completed with the MinElute Kit (Qiagen) and fragments were barcoded with dual indexes (Illumina Nextra). Paired-end sequencing (2 × 75-bp reads) was carried out using the Illumina NextSeq 500. Raw sequencing data were processed and aligned to the GRC37/hg19 reference genome using Bowtie 2 and regions of significant enrichment were identified using MACS v1.4.2. Merged peak lists were created using BedTools. ATAC sequencing tag enrichment and DNA motif analysis across the merged peak list were carried out using HOMER (http://homer.salk.edu). Gene Ontology pathway analysis was performed with Metascape (http://metascape.org). Only high-confidence peaks were used for gene ontology and DNA motif analyses. For these evaluations, peaks with an enrichment score less than 5 were filtered out as previously established[39].

CAR T cell differentiation and expansion potency assays. Bulk primary human T cells were activated with paramagnetic beads coated with anti-CD3 and anti-CD28 monoclonal antibodies as previously described[40] and transduced with lentiviral vectors encoding the CD19BBζ CAR and shRNA hairpin sequences targeting *TET2* or a scrambled control with GFP co-expression (Cellecta). Knockdown efficiency in CTL019 cells following shRNA transduction was determined by real-time quantitative PCR with Taqman gene expression assays (Applied Biosystems) for TET2 (assay Hs00325999_m1) and GAPDH (assay (Hs03929097_g1), which served as a loading and normalization control. Following 14 days of culture, the differentiation phenotype of these cells was determined by flow cytometry. GFP^+CAR^+ T cells were sorted on a FACSAria (BD) and combined 1:1 with irradiated K562 cells engineered to express CD19[4] or mesothelin as a negative control. CTL019 cells were serially re-stimulated with irradiated K562 targets three times, with absolute counts and viability assessments taken at regular intervals over 17 days. Cell counts and viability measurements were obtained using the LUNA Automated Cell Counter (Logos Biosystems). Supernatants were collected 24 h after each stimulation for longitudinal measurements of cytokine levels in cultures, as previously described[41].

Intracellular cytokine, perforin and granzyme B analysis. $CD8^+$ T cells from Patient-10 were stimulated 3:1 with paramagnetic beads coated with anti-CD3 and anti-CD28 monoclonal antibodies for 6 h in the presence of CD107a monoclonal antibody and the golgi inhibitors brefeldin A and monensin. Cells were washed and stained with live/dead viability dye, followed by surface staining for CD3, CD8 and TCRVβ5.1. These lymphocytes were subsequently fixed/permeabilized and intracellularly stained for IFNγ. CAR T cells generated from healthy donors (TET2 knockdown or control) were stimulated in the same way with CD3/CD28 beads or beads coated with an anti-idiotypic antibody against CAR19. Cells were then stained for surface antigens (CD3, CD4, CD8 and CAR19). After fixation and permeabilization, intracellular staining for IFNγ, TNFα and IL-2 was performed.

For perforin and granzyme B analysis, CTL019 cells that had been transduced with a *TET2* or scrambled control shRNA were expanded for 14 days and cryopreserved. These CAR T cells were then thawed and rested for 4 h, followed by live/dead and surface staining for CD3, CD8 and CAR19. Intracellular staining for perforin and granzyme was carried out following fixation and permeabilization. Cells were analysed on an LSRFortessa (BD).

Cytotoxicity assay. Healthy donor CTL019 cells transduced with a shRNA directed against *TET2* or a scrambled control were co-cultured with CBG luciferase-expressing NALM-6 and OSU-CLL cell lines at the indicated ratios for 16 h[41]. Cell extracts were created using the Bright-Glo Luciferase Assay System (Promega Corporation) and substrate was added according to the manufacturer's instructions. Luciferase measurements were taken on a SpectraMax luminescence microplate reader (Molecular Devices), and specific lysis was calculated as previously described[41].

Analysis of *TET2* gene expression levels in T cell subsets. *TET2* expression levels were determined by analysing a published gene expression dataset (https://www.ncbi.nlm.nih.gov/geo/query/acc.cgi?acc=GSE23321) for $CD8^+$ T cell subsets (naive, stem cell memory, central memory and effector memory) isolated from three healthy human subjects[42]. Genechip (Affymetrix) data were processed with the Bioconductor Oligo software package[43] (release 3.6, Bioconductor) using the RMA method[44].

Statistical analyses. Normality was assessed for all data using the D'Agostino–Pearson omnibus test. For integration site data analysis, genomic feature data comparisons were carried out as previously described using χ^2, Fisher's exact tests, or a combination of Bayesian model averaging, conditional logit and regression[27,45,46]. Assessments of T cell differentiation and function in shRNA-mediated *TET2* knockdown experiments were performed using a paired Student's *t*-test. Estimates of variation within each group of data are presented as error bars. Analyses were performed with SAS (SAS Institute), Stata 13.0 (StataCorp) or GraphPad Prism 6 (GraphPad Software). Cytokine heat maps were constructed using Morpheus software (Broad Institute; accessed at https://software.broadinstitute.org/morpheus/). All tests were two-sided. Exact *P* values are reported. $P < 0.05$ was considered statistically significant.

Reporting summary. Further information on experimental design is available in the Nature Research Reporting Summary linked to this paper.

Data availability. Sequencing data are available at the NCBI Sequence Read Archive (accession number SRP136348; analyses of lentiviral integration sites, TET2 chimaeric transcripts and alleles as well as mutations associated with hematologic malignancies), Adaptive Biotechnologies' immuneACCESS database (https://doi.org/10.21417/B72D1Q; TCRVβ and BCR IgH immunosequencing) and Gene Expression Omnibus (accession number GSE112494; ATAC–seq). Any other data that support the findings of the study will be made available upon reasonable request.

22. Hertlein, E. et al. Characterization of a new chronic lymphocytic leukemia cell line for mechanistic in vitro and in vivo studies relevant to disease. *PLoS ONE* **8**, e76607 (2013).
23. Barrett, D. M. et al. Treatment of advanced leukemia in mice with mRNA engineered T cells. *Hum. Gene Ther.* **22**, 1575–1586 (2011).
24. Maude, S. L. et al. Chimeric antigen receptor T cells for sustained remissions in leukemia. *N. Engl. J. Med.* **371**, 1507–1517 (2014).
25. Jena, B. et al. Chimeric antigen receptor (CAR)-specific monoclonal antibody to detect CD19-specific T cells in clinical trials. *PLoS ONE* **8**, e57838 (2013).
26. Brady, T. et al. A method to sequence and quantify DNA integration for monitoring outcome in gene therapy. *Nucleic Acids Res.* **39**, e72 (2011).
27. Berry, C., Hannenhalli, S., Leipzig, J. & Bushman, F. D. Selection of target sites for mobile DNA integration in the human genome. *PLOS Comput. Biol.* **2**, e157 (2006).
28. Berry, C. C. et al. Estimating abundances of retroviral insertion sites from DNA fragment length data. *Bioinformatics* **28**, 755–762 (2012).
29. Berry, C. C., Ocwieja, K. E., Malani, N. & Bushman, F. D. Comparing DNA integration site clusters with scan statistics. *Bioinformatics* **30**, 1493–1500 (2014).
30. Scholler, J. et al. Decade-long safety and function of retroviral-modified chimeric antigen receptor T cells. *Sci. Transl. Med.* **4**, 132ra53 (2012).
31. Daber, R., Sukhadia, S. & Morrissette, J. J. Understanding the limitations of next generation sequencing informatics, an approach to clinical pipeline validation using artificial data sets. *Cancer Genet.* **206**, 441–448 (2013).
32. Liu, M. Y. et al. Mutations along a TET2 active site scaffold stall oxidation at 5-hydroxymethylcytosine. *Nat. Chem. Bio.* **13**, 181–187 (2017).
33. Hu, L. et al. Crystal structure of TET2-DNA complex: insight into TET-mediated 5mC oxidation. *Cell* **155**, 1545–1555 (2013).
34. Liu, M. Y., DeNizio, J. E. & Kohli, R. M. Quantification of oxidized 5-methylcytosine bases and TET enzyme activity. *Methods Enzymol.* **573**, 365–385 (2016).
35. Jin, J. et al. Simplified method of the growth of human tumor infiltrating lymphocytes in gas-permeable flasks to numbers needed for patient treatment. *J. Immunother.* **35**, 283–292 (2012).
36. Carty, S. A. et al. The loss of TET2 promotes $CD8^+$ T cell memory differentiation. *J. Immunol.* **200**, 82–91 (2018).
37. Buenrostro, J. D., Giresi, P. G., Zaba, L. C., Chang, H. Y. & Greenleaf, W. J. Transposition of native chromatin for fast and sensitive epigenomic profiling of open chromatin, DNA-binding proteins and nucleosome position. *Nat. Methods* **10**, 1213–1218 (2013).
38. Pauken, K. E. et al. Epigenetic stability of exhausted T cells limits durability of reinvigoration by PD-1 blockade. *Science* **354**, 1160–1165 (2016).
39. Xu, J. et al. Landscape of monoallelic DNA accessibility in mouse embryonic stem cells and neural progenitor cells. *Nat. Genet.* **49**, 377–386 (2017).
40. Laport, G. G. et al. Adoptive transfer of costimulated T cells induces lymphocytosis in patients with relapsed/refractory non-Hodgkin lymphoma following $CD34^+$-selected hematopoietic cell transplantation. *Blood* **102**, 2004–2013 (2003).
41. Fraietta, J. A. et al. Ibrutinib enhances chimeric antigen receptor T cell engraftment and efficacy in leukemia. *Blood* **127**, 1117–1127 (2016).
42. Gattinoni, L. et al. A human memory T cell subset with stem cell-like properties. *Nat. Med.* **17**, 1290–1297 (2011).
43. Carvalho, B. S. & Irizarry, R. A. A framework for oligonucleotide microarray preprocessing. *Bioinformatics* **26**, 2363–2367 (2010).
44. Irizarry, R. A. et al. Summaries of Affymetrix GeneChip probe level data. *Nucleic Acids Res.* **31**, e15 (2003).
45. Brady, T. et al. Integration target site selection by a resurrected human endogenous retrovirus. *Genes Dev.* **23**, 633–642 (2009).
46. Ocwieja, K. E. et al. HIV integration targeting: a pathway involving Transportin-3 and the nuclear pore protein RanBP2. *PLoS Pathog.* **7**, e1001313 (2011).
47. Moskowitz, D. M. et al. Epigenomics of human CD8 T cell differentiation and aging. *Sci. Immunol.* **2**, eaag0192 (2017).

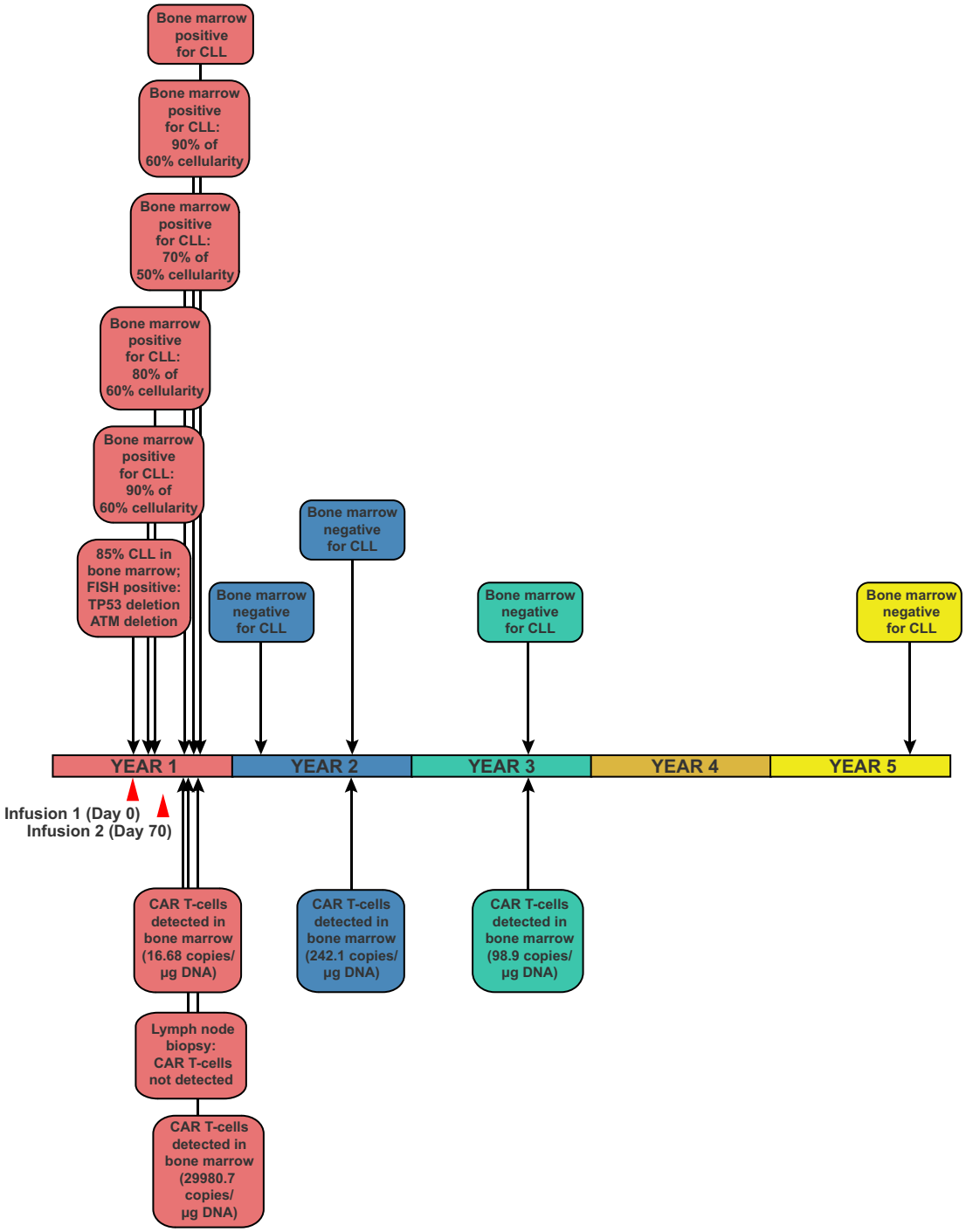

Extended Data Fig. 1 | Timeline of disease clearance by CAR T cells in Patient-10. An outline of clinical findings in Patient-10, including the results of bone marrow assessments, tumour cytogenetics and CAR T cell persistence. CTL019 cell infusion time points are indicated by red arrows.

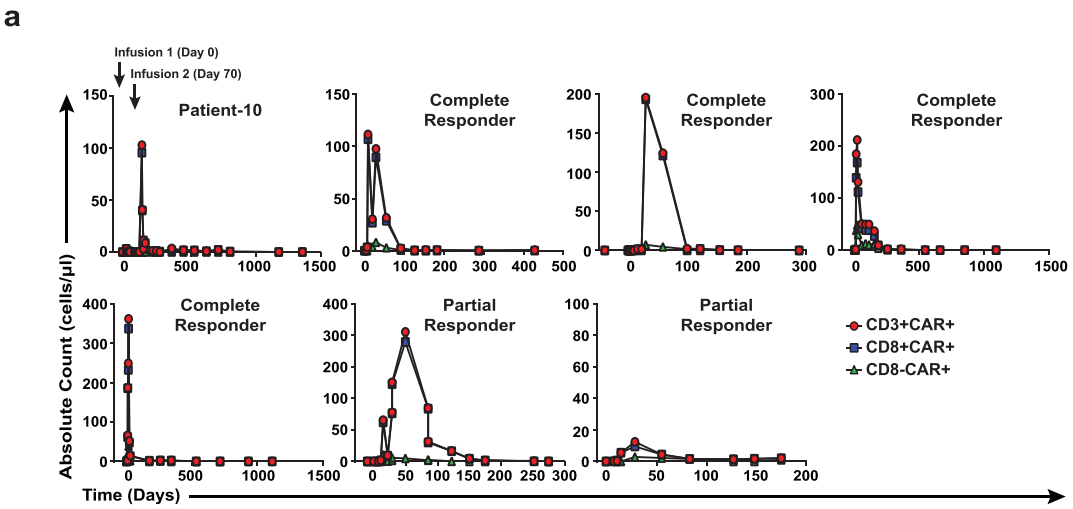

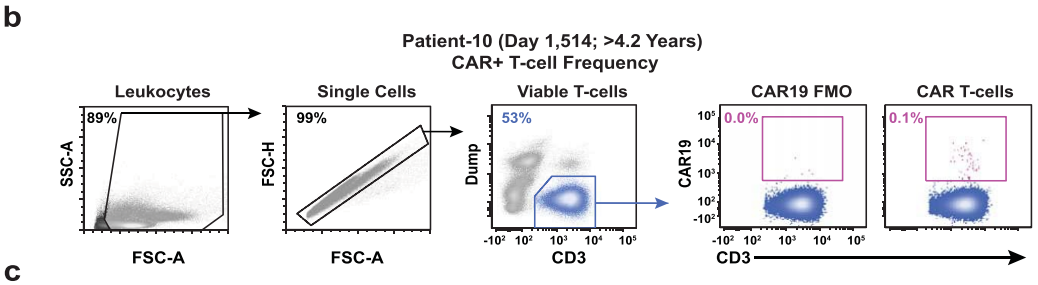

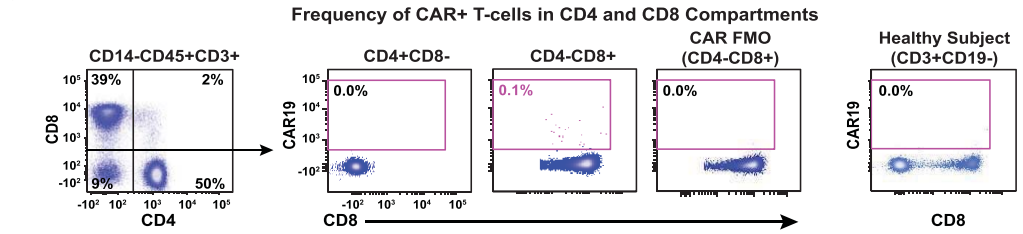

d

qPCR-Based Detection of CAR19 in the Peripheral Blood

Average Ct	SD	Average Marking/Cell (%)	Copies/µg DNA
33.56	0.09	0.0860	136.54

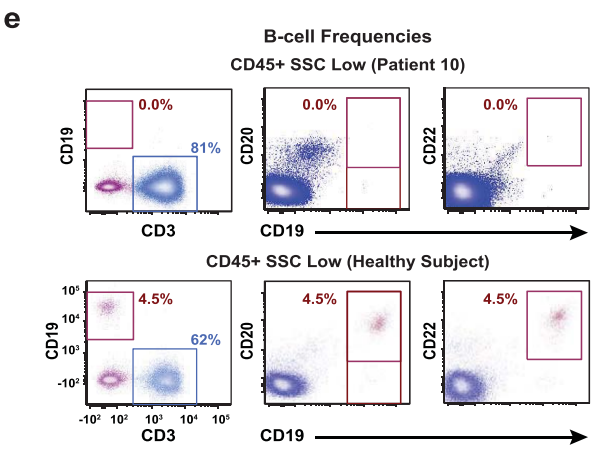

f

Enumeration of Peripheral Blood Cells

Cell Population	Frequency (%)
CD45+CD14-	65
CD3+ (Live/Dead Dye-)	53
CD3+CD8+	39
CD3+CD4+	51
CD3+CD4+CD8+	2
CD3-CD56+	16
CD3+CD56+	2
CD3+HLA-DR+	5
CD3+CD4+CD8-HLA-DR+	6
CD3+CD4-CD8+HLA-DR+	3
γδ TCR+	9
γδ TCR+CD4+	0.75
γδ TCR+CD8+	8
CD3+CAR19+	0.1
CD3+CD4+CAR19+	0
CD3+CD8+CAR19+	0.1
CD3+HLA-DR+CAR19+	0
γδ TCR+CAR19+	0
CD19+	0

Extended Data Fig. 2 | See next page for caption.

Extended Data Fig. 2 | CAR T cell detection and profiling of immune cell populations in Patient-10 and other responders. a, Pre- and post-infusion kinetics of CAR T cell expansion ($CD3^+$, $CD8^+$ and $CD8^-$) are shown in Patient-10 compared to other responders. The number of circulating CTL019 cells was calculated based on frequencies of $CD3^+$, $CD8^+$ and $CD8^-$ CAR T cell populations and absolute cell counts. **b**, Flow cytometry gating strategy to identify peripheral blood CAR T cells in Patient-10. **c**, Relative percentages of CTL019 cells in the CD4 and CD8 compartments of this patient. T cells from a healthy subject served as a negative control. **d**, The persistence of CAR T cells in the peripheral blood of Patient-10 was determined by qPCR. The average threshold cycle (*Ct*) value obtained from three replicates and a standard deviation (SD) is listed. Calculations of CAR T cell abundance are reported as average marking per cell as well as transgene copies per microgram of genomic DNA. **e**, Frequencies of circulating B cells in Patient-10 compared to a healthy subject. Pre-gating was performed to exclude dead cells as well as doublets, and all gating thresholds were based on fluorescence minus one (FMO) controls (representative of two independent experiments). **f**, Enumeration of various immune cell populations in the blood of Patient-10. The frequency of each population is listed in a separate column that corresponds to its phenotypic marker.

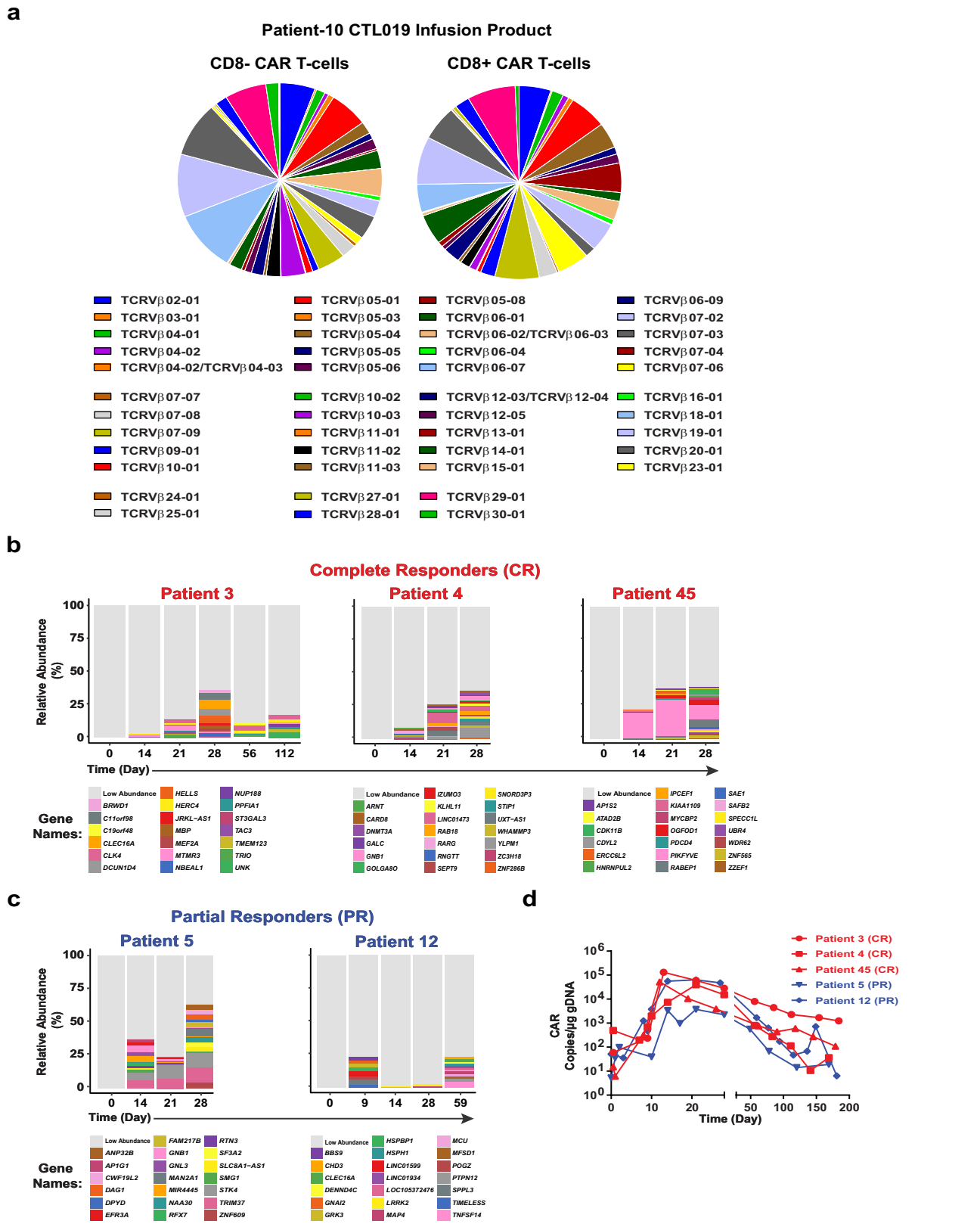

Extended Data Fig. 3 | Clonal composition of CAR T cells from Patient-10 and other subjects treated with CTL019. a, TCRVβ distribution in CD8$^-$ (left) and CD8$^+$ (right) CAR T cells in the cellular infusion product of Patient-10. **b**, Relative frequencies of CAR T cell clones in three patients who had complete responses to CTL019 therapy, summarized as stacked bar graphs. Each colour (horizontal bar) denotes a major cell clone, as marked by lentiviral integration sites. **c**, Integration site analysis in CAR T cells from two partially responding patients. **d**, In vivo expansion of CAR T cells in the above patients as determined by quantifying the average CAR transgene copies per microgram DNA at each time point.

a

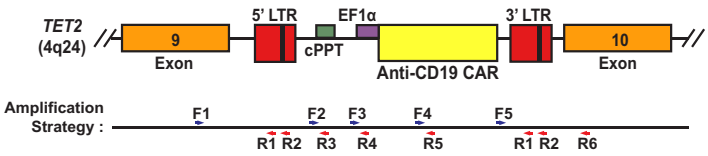

Primer	Target	Direction	Sequence
F1	TET2 exon 9	Forward	GACTTGCACAACATGCAGAA
R6	TET2 exon 10	Reverse	GTATAAAGGCAGAACGTGAAGC
R1	Vector R element	Reverse	AGCAGTGGGTTCCCTAGTTA
R3	Vector cPPT element	Reverse	TGCCATTTGTACTGCTGTCTTA
R4	Vector EF1α promoter	Reverse	CAAGGGCCATAACCCGTAAA
R5	Vector 4-1BB region (CAR)	Reverse	GCCATCTTCCTCTTGAGTAGTT
R2	Vector LTR poly(A) signal	Reverse	GGCAAGCTTTATTGAGGCTT
F2	Vector cPPT element	Forward	AGGAATTTGGCATTCCCTACA
F3	Vector EF1α promoter	Forward	GGAGAACCGTATATAAGTGCAGTAG
F4	Vector 4-1BB region (CAR)	Forward	CCTTCTCCTGTCACTGGTTATC
F5	Vector R element	Forward	GAAGGGCTAATTCACTCCCAA

Chimera	Splice Site	Donor Sequence	Acceptor Sequence
1	1st	ACAUUG | GUAAGU	CUCUAG | CAGUGG
1	2nd	GACUGG | UGAGUA	GUUAGG | CAGGGA
2	1st	ACAUUG | GUAAGU	UUUCAG | GUGUCG
3	1st	ACAUUG | GUAAGU	UAACAG | GUAGGA
3	2nd	CAACUA | AUGUAG	GGGGAC | UGGAAG

b

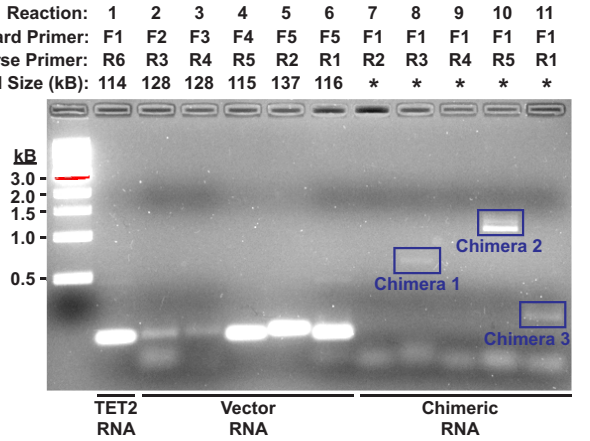

Reaction Targets

1: *TET2* exon 9 and 10 junction
2: Vector cPPT element
3: Vector EF1α promoter
4: Vector 4-1BB region (CAR)
5: Vector LTR U5 region
6: Vector LTR R region
7: *TET2* exon 9 to LTR U5 region
8: *TET2* exon 9 to cPPT element
9: *TET2* exon 9 to EF1α promoter
10: *TET2* exon 9 to 4-1BB region (CAR)
11: *TET2* exon 9 to LTR R region

c

Next-Generation Sequencing Multi-Gene Mutation Panel

Hematologic Malignancies

ABL1	*CEBPA*	*GATA2*	*MAP2K1*	*NPM1*	*RUNX1*	*TP53*
ASXL1	*CSF1R*	*GNAS*	*MAPK1*	*NRAS*	*SETBP1*	*TPMT*
ATM	*CSF3R*	*HNRNPK*	*MIR142*	*PDGFRA*	*SF1*	*U2AF1*
BCOR	*DDX3X*	*IDH1*	*MPL*	*PHF6*	*SF3A1*	*U2AF2*
BCORL1	*DNMT3A*	*IDH2*	*MYC*	*POT1*	*SF3B1*	*WT1*
BIRC3	*ETV6*	*IL7R*	*MYCN*	*PRPF40B*	*SMC1A*	*XPO1*
BRAF	*EZH2*	*JAK2*	*MYD88*	*PTEN*	*SRSF2*	*ZMYM3*
CALR	*FAM5C*	*KIT*	*NF1*	*PTPN11*	*STAG2*	*ZRSR2*
CBL	*FBXW7*	*KLHL6*	*NOTCH1*	*RAD21*	*TBL1XR1*	
CDKN2A	*FLT3*	*KRAS*	*NOTCH2*	*RIT1*	*TET2*	

d

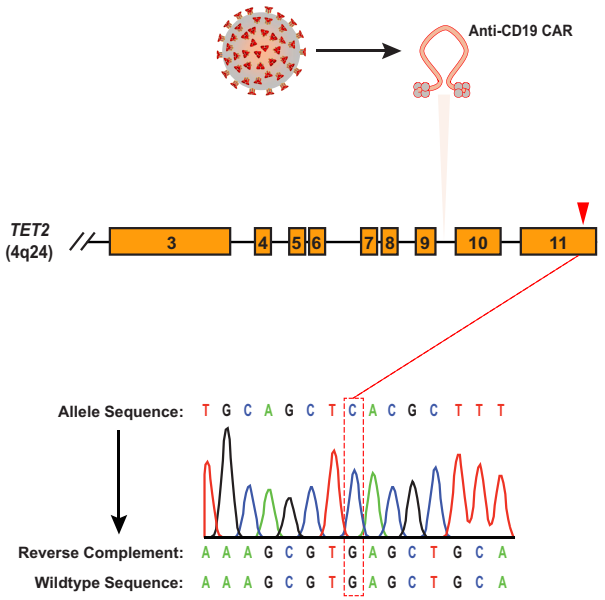

Extended Data Fig. 4 | Detection of *TET2* chimaeric transcripts in Patient-10 CAR T cells and DNA sequencing for mutation detection. **a**, The strategy for detection of polyadenylated RNA corresponding to truncated *TET2* transcripts is depicted. Boxes represent the genomic regions between *TET2* exons 9 and 10 with the integrated vector present. Blue and red arrows indicate general locations of the forward and reverse primers, which are listed below the diagram. LTR, long terminal repeat; cPPT, polypurine tract; EF1α, elongation factor 1-α promoter. Sequences corresponding to the splice junctions for the three chimaeric messages (five total junctions) are listed in the bottom chart. Underlines indicate consensus splice donors and acceptors. **b**, Visualization of chimaeric *TET2* RT–PCR products. PCR products were separated on a native agarose gel and stained with ethidium bromide. Expected sizes of amplicons are listed above the gel. Truncated transcripts are highlighted by blue boxes. A key to the RT–PCR reactions is shown below the diagram. *Band size not determined (two independent experiments). **c**, Genes interrogated by the next generation sequencing panel used to analyse DNA isolated from $CD8^{+}CAR^{+}$ T cells and CAR^{-} T cells in Patient-10 at the peak of his response. **d**, Sanger sequencing of specific amplifications corresponding to the allele that was disrupted by integration of the CAR lentivirus is shown. The mutation that was detected by next generation sequencing of total genomic DNA from CAR^{+} T cells (Fig. 3c) is not present in the *TET2* allele hosting the lentiviral integration site.

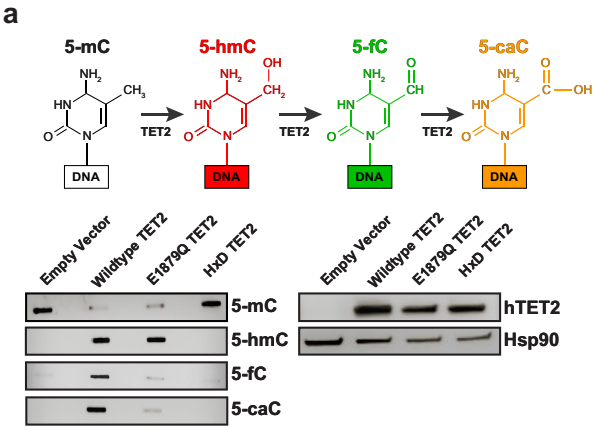

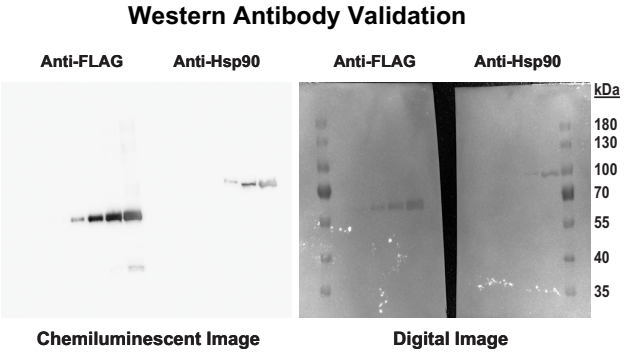

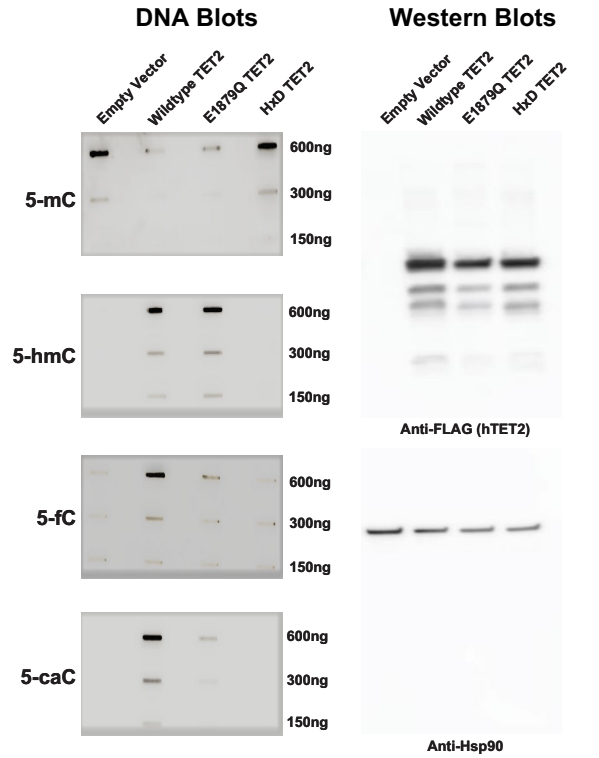

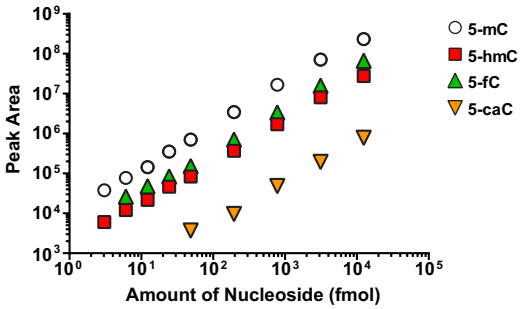

e

Raw and Normalized LC-MS/MS Data

Peak Areas	5-mC	5-hmC	5-fC	5-caC
Empty Vector (1)	20,156,324	-	-	-
Empty Vector (2)	11,963,548	-	-	-
Empty Vector (3)	12,508,852	-	-	-
Wildtype TET2 (1)	3,129,967	61,498	238,426	2,921
Wildtype TET2 (2)	6,442,997	85,691	331,456	2,101
Wildtype TET2 (3)	7,787,826	84,194	314,389	2,713
E1879Q TET2 (1)	14,350,779	170,991	404,648	4,008
E1879Q TET2 (2)	7,080,722	84,132	166,821	-
E1879Q TET2 (3)	7,228,118	74,472	129,216	1,736
HxD TET2 (1)	16,137,499	-	-	-
HxD TET2 (2)	12,183,964	-	-	-

Normalized Amounts (fmol)	5-mC	5-hmC	5-fC	5-caC	Total (fmol)
Empty Vector (1)	1,066	-	-	-	1,066
Empty Vector (2)	633	-	-	-	633
Empty Vector (3)	661	-	-	-	661
Wildtype TET2 (1)	166	18	45	47	275
Wildtype TET2 (2)	341	24	63	34	461
Wildtype TET2 (3)	412	24	59	43	539
E1879Q TET2 (1)	759	49	76	64	948
E1879Q TET2 (2)	374	24	31	-	430
E1879Q TET2 (3)	382	21	24	28	456
HxD TET2 (1)	853	-	-	-	853
HxD TET2 (2)	644	-	-	-	644

% of Modified Cytosines	5-mC	5-hmC	5-fC	5-caC
Empty Vector (1)	100	0	0	0
Empty Vector (2)	100	0	0	0
Empty Vector (3)	100	0	0	0
Wildtype TET2 (1)	60	6	16	17
Wildtype TET2 (2)	74	5	14	7
Wildtype TET2 (3)	76	4	11	8
E1879Q TET2 (1)	80	5	8	7
E1879Q TET2 (2)	87	6	7	0
E1879Q TET2 (3)	84	5	5	6
HxD TET2 (1)	100	0	0	0
HxD TET2 (2)	100	0	0	0

Extended Data Fig. 5 | See next page for caption.

Extended Data Fig. 5 | Analysis of DNA methylation variants from HEK293T cells overexpressing TET2. a, Depiction of sequential oxidations of 5-mC to 5-hmC, 5-fC and 5-caC catalysed by TET2 (top). Dot blots for 5-mC, 5-hmC, 5-fC and 5-caC in genomic DNA (gDNA) isolated from HEK293T cells transfected with the E1879Q TET2 mutant are shown. Assay controls include an empty vector, wild-type TET2 and a catalytically inactive (HxD) TET2 mutant (bottom left). A western blot using anti-FLAG antibody to detect hTET2 in the above cells is also shown. Hsp90α/β was used as a loading control (bottom right). Brightness and contrast were adjusted evenly across blots. **b**, Original, uncropped DNA (left) and western (right) blots. A dilution series was used for semiquantitative analysis of DNA methylation variants. Representative results of three independent experiments are shown. **c**, Validation of anti-FLAG and anti-Hsp90α/β antibodies. Serial dilutions of lysates (0.008, 0.04, 0.2, 0.8, 4.0 $\mu g\ \mu l^{-1}$) obtained from HEK293T cells transfected with wild-type TET2. Gels were probed by western blot. Both chemiluminescence (left) and digital (right) images were captured, demonstrating that these antibodies exhibit specificity for the expected FLAG tag and Hsp90 based on molecular weight markers. **d**, 5-mC, 5-hmC, 5-fC and 5-caC nucleosides were analysed at fixed concentrations using LC–MS/MS to generate standard curves. The area under the curve (AUC) was calculated for each MS/MS fragment. In the case of 5-hmC, the slope was further adjusted because of quality control analysis of an equimolar mixture of oligonucleotides, each containing a single modification. **e**, Analysis of gDNA from individual biological replicates within each HEK293T cell group. The top chart lists the raw AUCs that were converted to relative amounts of modified cytosine (middle) according to their signal intensities from the respective standard curves. The percentage of each modified cytosine calculated for each sample is shown in the bottom chart. Results are from three independent experiments.

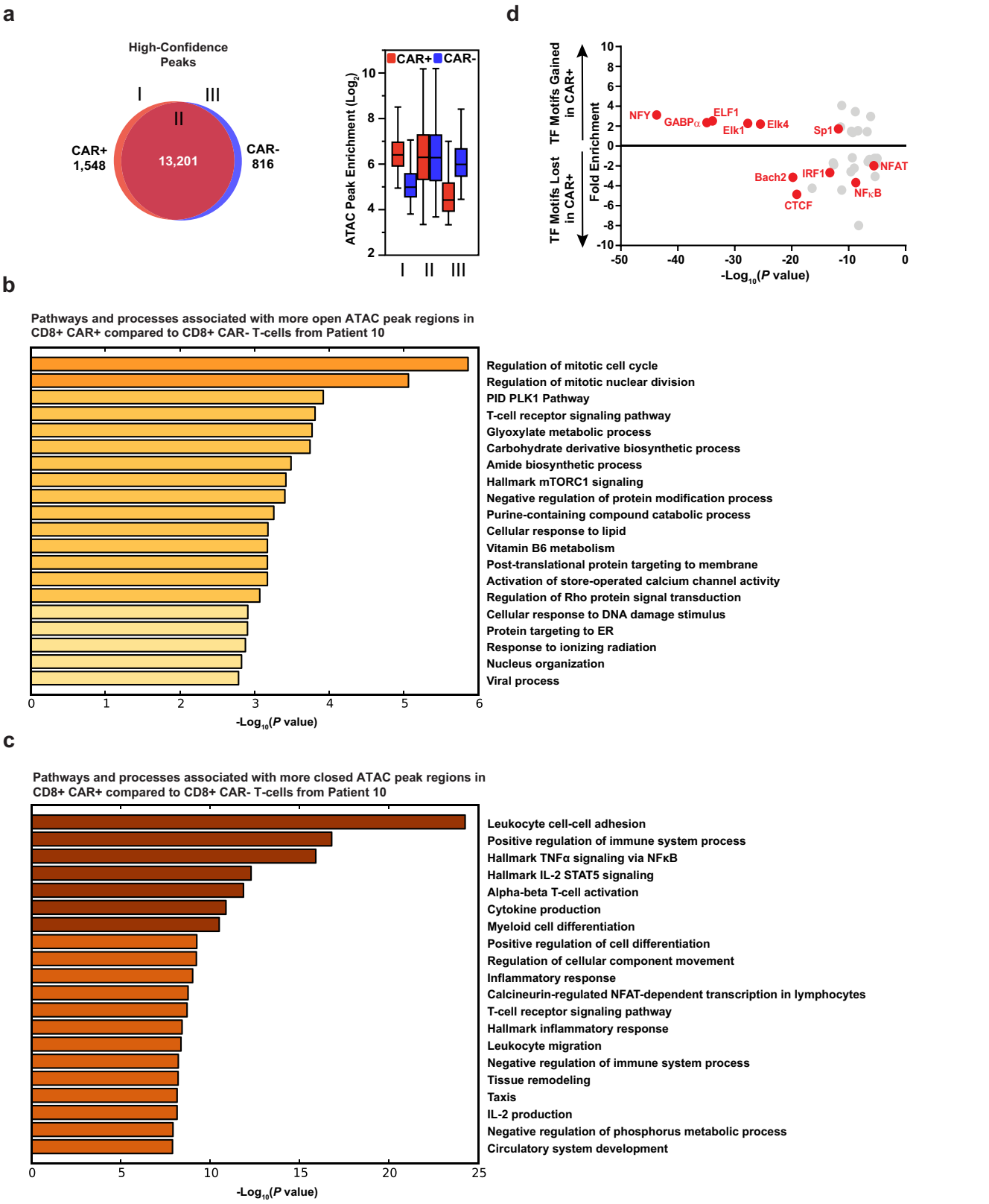

Extended Data Fig. 6 | See next page for caption.

Extended Data Fig. 6 | Global chromatin profiling of CAR$^+$ and CAR$^-$ T cells from Patient-10. a, Venn diagrams of high-confidence differential ATAC–seq regions (left) and enrichment of those peaks in regions of the diagrams (right) in CAR$^+$ and CAR$^-$CD8$^+$ T cells expanded from Patient-10 (two biological replicates analysed in two independent experiments). Boxes extend from the 25th to 75th percentiles, the middle line denotes the median and whiskers show minimum and maximum. **b**, Gene Ontology terms associated with chromatin regions that are significantly more open in CD8$^+$CAR$^+$ T cells from Patient-10 compared to their matched CD8$^+$CAR$^-$ T cell counterparts. **c**, Ontology analysis for chromatin regions that are less accessible in CD8$^+$CAR$^+$ T cells than in CD8$^+$CAR$^-$ T cells. **d**, Enrichment of transcription factor (TF) binding motifs in chromatin regions gained or lost in CAR$^+$ compared to CAR$^-$ T cells from Patient-10. Transcription factor motifs that were potentially more accessible in increased ATAC–seq peaks of CAR$^+$ T cells included E26 transformation-specific (ETS) (GABPα, ELF1, Elk4) and zinc finger (ZF) transcription factor (Sp1) binding sites that are known to be enriched in human CD8$^+$ T cells before differentiation occurs[47]. Transcription factor motifs that were potentially less accessible owing to reduced ATAC–seq peaks in CAR$^+$ T cells from Patient 10 (NF-κB, IRF1, NFAT–AP1 and CTCF) are enriched in terminally differentiated effector and exhausted T cells and have known key roles in forming the epigenetic landscape that programs their biology[38].

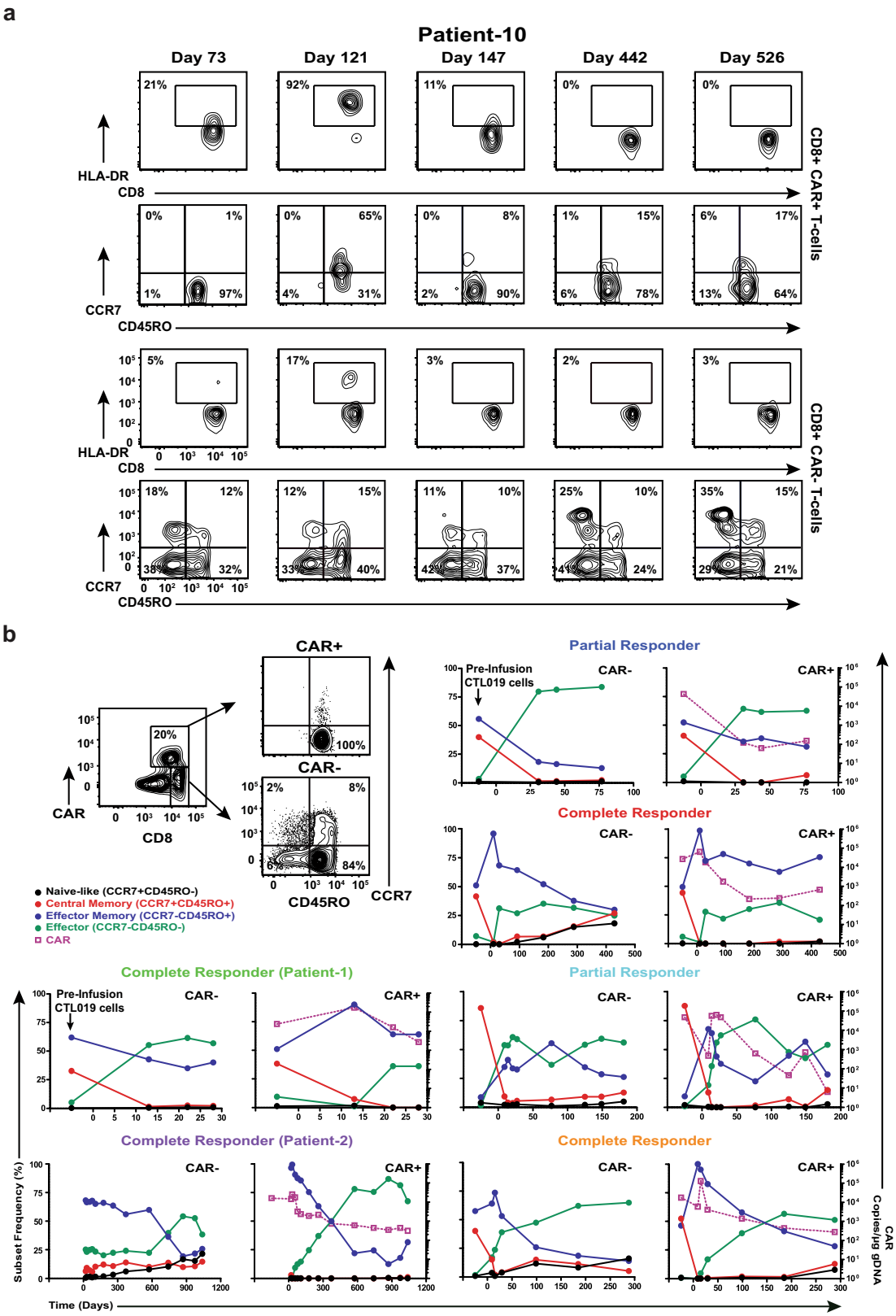

Extended Data Fig. 7 | The differentiation state of CAR T cells in Patient-10 compared to other responders over time. a, Representative contour plots of flow cytometric data depicting the frequency of CAR^+ and CAR^-CD8^+ T cells in Patient-10 that express HLA-DR. The proportions of these cells that express CD45RO and CCR7 as determinants of differentiation status are shown. Contour plot insets indicate the frequencies of the gated cell populations. **b**, Example gating strategy used to determine the differentiation phenotype of $CD8^+CAR^+$ and CAR^- T cells from a complete responder (top left). Line graphs depict the differentiation state of these cell populations in other responding patients over time and are plotted with corresponding CAR T cell levels in the blood, as determined by qPCR.

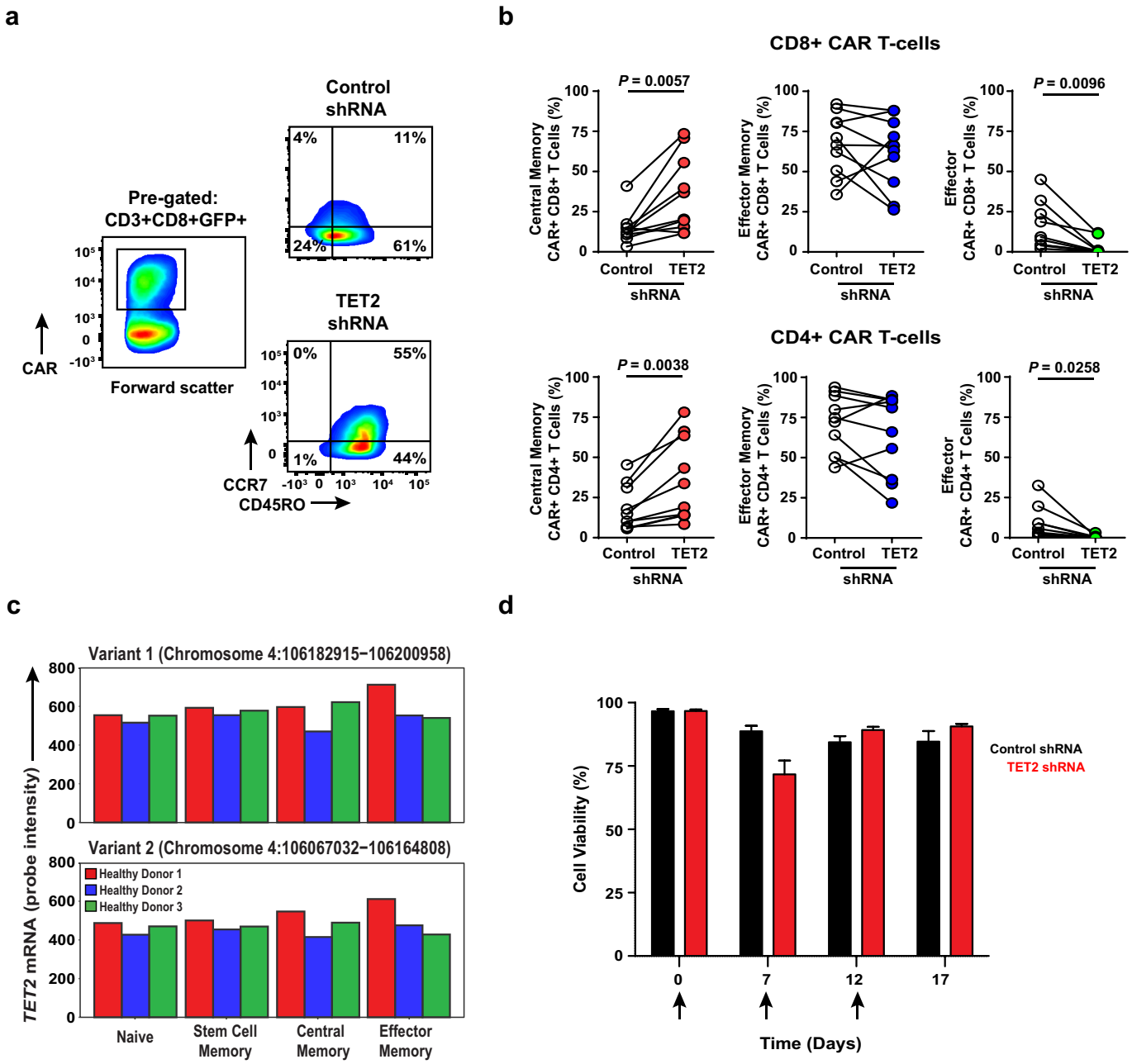

Extended Data Fig. 8 | Effect of TET2 expression on T cell differentiation and viability. a, Representative flow cytometry plots showing the differentiation state of healthy donor $CD8^+CAR^+$ T cells after transduction with a scrambled shRNA (control) or shRNA targeting *TET2*. Insets define frequencies of gated populations. **b**, Frequencies of healthy subject CAR^+CD8^+ (top) and CAR^+CD4^+ (bottom) T cells according to differentiation phenotype following control or *TET2* shRNA transduction ($n = 10$; pooled results from four independent experiments). *P* values were determined using a two-tailed, paired Student's *t*-test. **c**, Comparison of the expression levels of *TET2* in naive and memory $CD8^+$ T cell subsets from three healthy donors. Two variants encoding different isoforms have been identified for this gene in humans. Expression levels of each *TET2* variant were estimated by measuring the probe intensity from microarray analysis. **d**, Viability of CAR^+ T cells transduced with a *TET2* shRNA or scrambled control and restimulated with K562 cells expressing CD19 ($n = 12$; pooled results from three independent experiments). Each arrow indicates the time point at which CAR T cells were exposed to antigen. Error bars depict s.e.m.

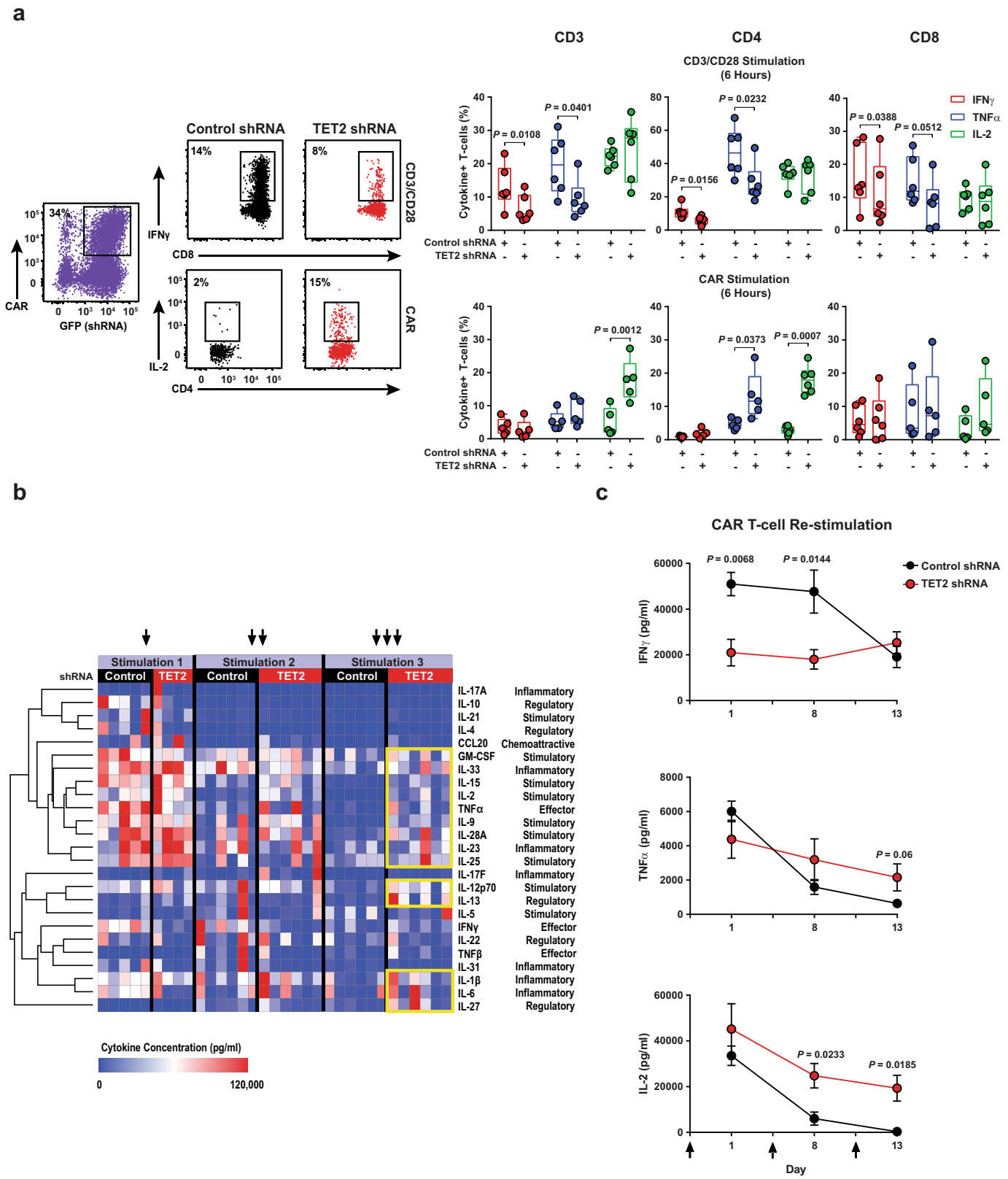

Extended Data Fig. 9 | See next page for caption.

Extended Data Fig. 9 | CAR T cell cytokine profiles following TET2 inhibition. a, Representative flow cytometry of acute intracellular cytokine production by healthy donor ($n = 6$; three independent experiments) CAR T cells transduced with a *TET2* shRNA or a scrambled control shRNA (left). Production of IFNγ, TNFα and IL-2 by total $CD3^+$, $CD4^+$ and $CD8^+$ CAR T cells is shown. These cells were stimulated with beads coated with anti-CD3 and anti-CD28 antibodies (top right) or CAR anti-idiotypic antibodies (bottom right). Boxes represent the 25th to 75th percentiles, the middle line denotes the median and whiskers depict minimum and maximum. **b**, Heat map and cluster analysis of cytokine profiles for CAR T cells transduced with a *TET2* shRNA or scrambled control and serially restimulated with irradiated K562 cells expressing CD19 are shown. Colours represent scaled cytokine data corresponding to each stimulation time point. Hierarchal clustering was used to generate the cluster dendrogram and cytokine response groups. **c**, Production of IFNγ (top), TNFα (middle) and IL-2 (bottom) by TET2 knockdown or control CAR T cells ($n = 6$; three independent experiments) following restimulation with CD19 antigen. Black arrows indicate when CAR T cells were exposed to CD19-expressing K562 cells. Error bars denote s.e.m. All *P* values were determined using a two-tailed, paired Student's *t*-test.

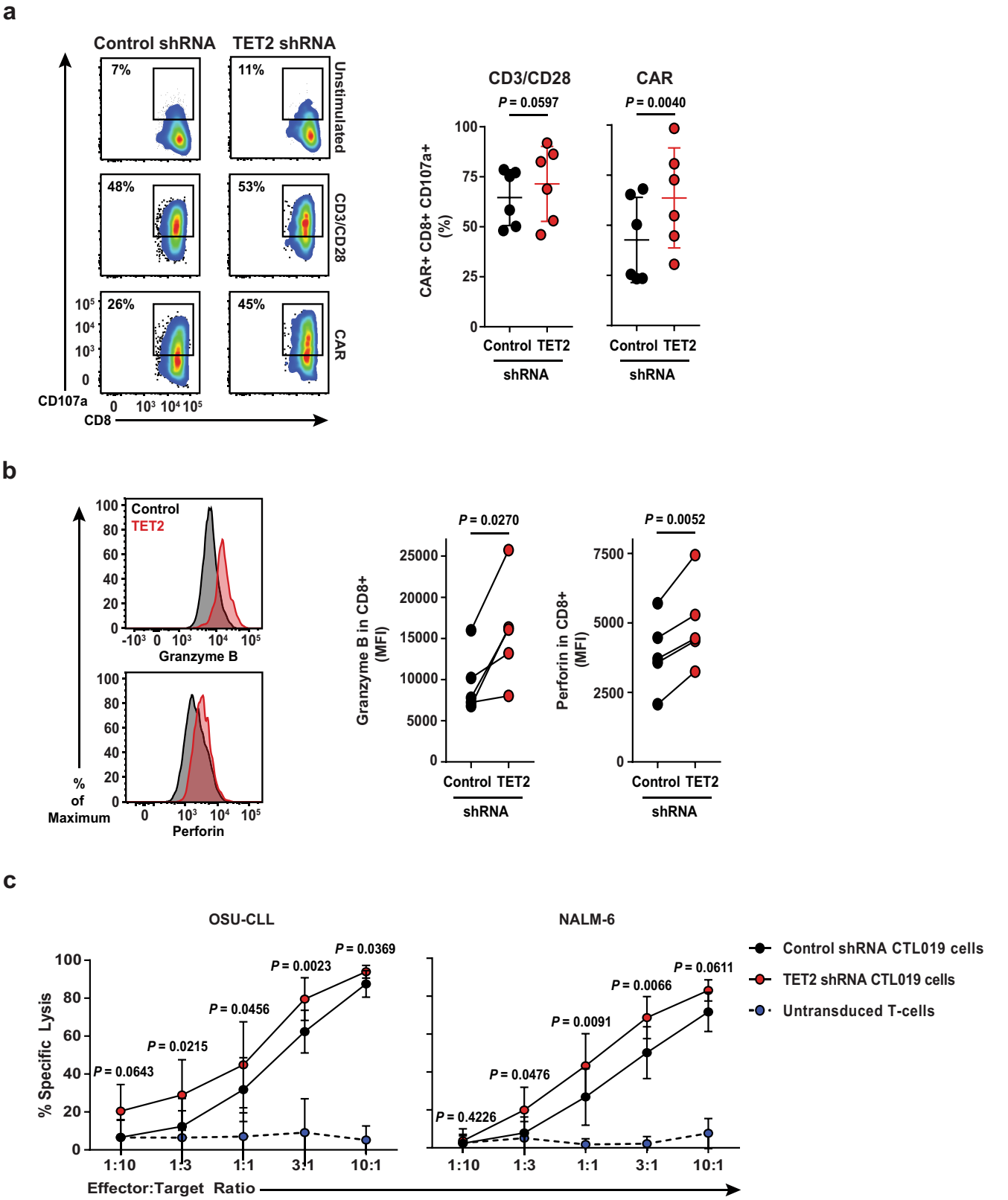

Extended Data Fig. 10 | Effect of *TET2* knockdown on the cytotoxic machinery of CAR T cells. a, Flow cytometry plots showing the frequency of *TET2* knockdown or control CAR T cells expressing CD107a (a marker of cytolysis) following CD3 and CD28 or CAR-specific stimulation (left). Summarized data from analysis of CAR T cells manufactured from $n = 6$ different healthy donors is shown (right). **b**, Representative histograms illustrating expression levels of granzyme B and perforin in CAR T cells in the setting of TET2 inhibition as compared to its counterpart control (left). Pooled data from CAR T cells of $n = 5$ healthy donors are summarized on the right. **c**, Cytotoxic capacity of CTL019 cells (transduced with a *TET2* or scrambled control shRNA) after overnight co-culture with luciferase-expressing OSU-CLL (left) or NALM-6 (right) cells. Untransduced T cells were included as an additional group to control for non-specific lysis. *P* values were determined using a two-tailed, paired Student's *t*-test. All data were pooled from three independent experiments.

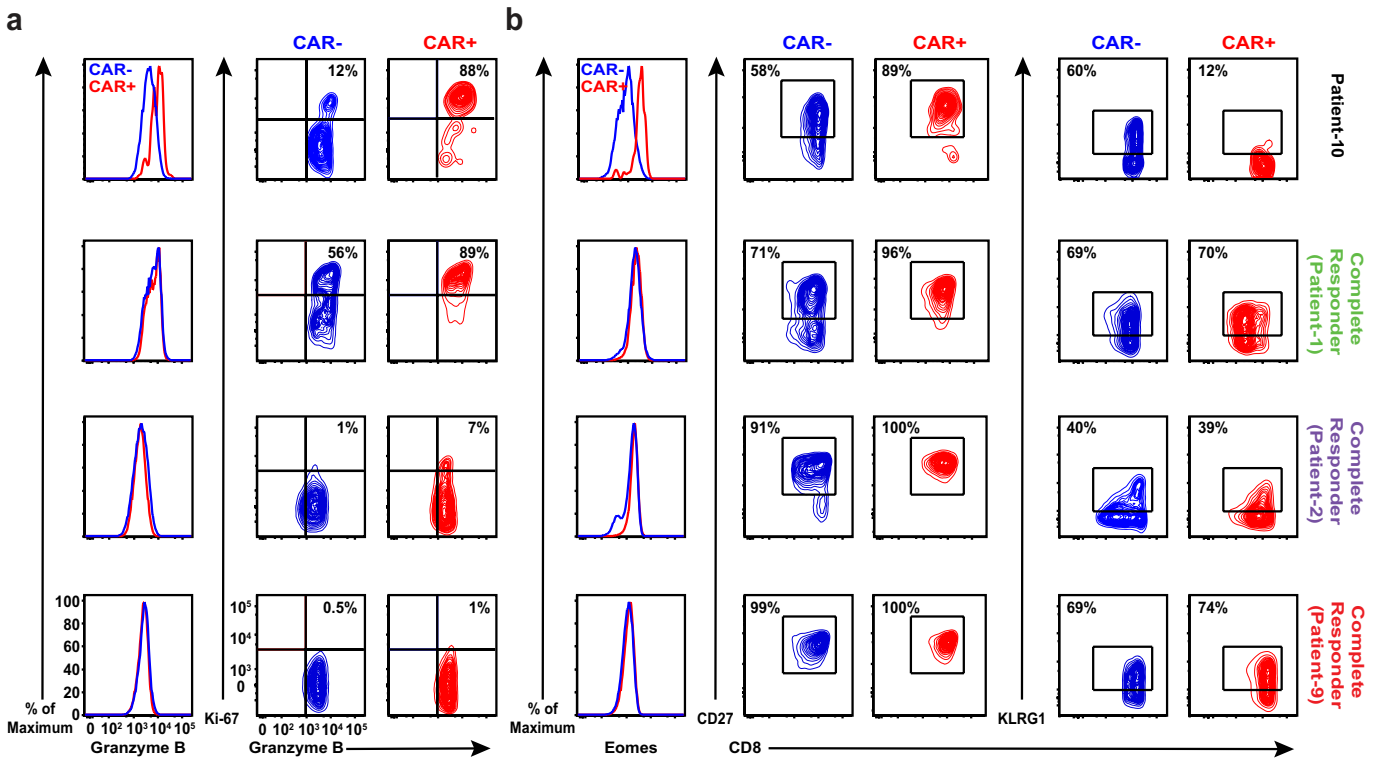

Extended Data Fig. 11 | Effector and memory molecule expression by CAR T cells from Patient-10 compared to those from other responding subjects. a, Expression of granzyme B (left) and the frequency of CAR^- and CAR^+ T cells co-expressing granzyme B/Ki-67 (right panel) at the peak of in vivo CTL019 expansion in Patient-10 compared to three other complete responders. **b**, Representative histograms of intracellular Eomes expression (left), and contour plots depicting frequencies of CD27- (middle) and KLRG1-expressing (right) lymphocytes in the same cell populations of these patients. These results are representative of three experiments repeated independently with comparable findings.

nature research

Corresponding author(s): Jan Joseph Melenhorst, Ph.D. and Carl H. June, M.D.

☐ Initial submission ☐ Revised version ☒ Final submission

Life Sciences Reporting Summary

Nature Research wishes to improve the reproducibility of the work that we publish. This form is intended for publication with all accepted life science papers and provides structure for consistency and transparency in reporting. Every life science submission will use this form; some list items might not apply to an individual manuscript, but all fields must be completed for clarity.

For further information on the points included in this form, see Reporting Life Sciences Research. For further information on Nature Research policies, including our data availability policy, see Authors & Referees and the Editorial Policy Checklist.

Experimental design

1. Sample size

Describe how sample size was determined.

The current study is a secondary investigation using patient samples collected from existing clinical trials. Therefore, the sample sizes in this report were determined by the original clinical trial designs and sample availability

2. Data exclusions

Describe any data exclusions.

Please see the above response. No additional inclusion/exclusion criteria were applied.

3. Replication

Describe whether the experimental findings were reliably reproduced.

All in vitro experiments were repeated with primary cells from different subjects in each separate experimental run. All attempts at replication of these experiments were successful.

4. Randomization

Describe how samples/organisms/participants were allocated into experimental groups.

The clinical trials were single-treatment studies; the comparison groups of patients in the current study were defined by the observed clinical responses.

5. Blinding

Describe whether the investigators were blinded to group allocation during data collection and/or analysis.

Investigators were blinded to clinical responses as correlative assays were conducted using de-identified subject samples.

Note: all studies involving animals and/or human research participants must disclose whether blinding and randomization were used.

6. Statistical parameters

For all figures and tables that use statistical methods, confirm that the following items are present in relevant figure legends (or in the Methods section if additional space is needed).

n/a	Confirmed	
☐	☒	The exact sample size (*n*) for each experimental group/condition, given as a discrete number and unit of measurement (animals, litters, cultures, etc.)
☐	☒	A description of how samples were collected, noting whether measurements were taken from distinct samples or whether the same sample was measured repeatedly
☐	☒	A statement indicating how many times each experiment was replicated
☐	☒	The statistical test(s) used and whether they are one- or two-sided (note: only common tests should be described solely by name; more complex techniques should be described in the Methods section)
☒	☐	A description of any assumptions or corrections, such as an adjustment for multiple comparisons
☐	☒	The test results (e.g. *P* values) given as exact values whenever possible and with confidence intervals noted
☐	☒	A clear description of statistics including central tendency (e.g. median, mean) and variation (e.g. standard deviation, interquartile range)
☐	☒	Clearly defined error bars

See the web collection on statistics for biologists for further resources and guidance.

Software

Policy information about availability of computer code

7. Software

Describe the software used to analyze the data in this study.	Flow cytometry data were analyzed using FlowJo software. For ATAC Seq. data, BedTools, HOMER and Metascape were used. Analysis of TCR VB and BCR IgH sequencing was done using the ImmunoSeq Analyzer.

For manuscripts utilizing custom algorithms or software that are central to the paper but not yet described in the published literature, software must be made available to editors and reviewers upon request. We strongly encourage code deposition in a community repository (e.g. GitHub). *Nature Methods* guidance for providing algorithms and software for publication provides further information on this topic.

Materials and reagents

Policy information about availability of materials

8. Materials availability

Indicate whether there are restrictions on availability of unique materials or if these materials are only available for distribution by a for-profit company.	B. Jena and L. Cooper (MD Anderson Cancer Center) provided the CAR anti-idiotype detection reagent.

9. Antibodies

Describe the antibodies used and how they were validated for use in the system under study (i.e. assay and species).	Information about flow cytometry antibodies can be found in the methods section. All clinical and research samples were analyzed in the Product Development and Correlative Sciences laboratories at the University of Pennsylvania and antibodies were validated in these laboratories. Western blot antibodies against FLAG and Hsp90 were validated using serial dilutions of HEK293T cell lysates as shown in Supplementary Figure 1c.

10. Eukaryotic cell lines

a. State the source of each eukaryotic cell line used.	NALM-6, K562 and HEK293T cell lines were originally obtained from the American Type Culture Collection (ATCC). The OSC-CLL line was derived and provided by investigators at Ohio State University.
b. Describe the method of cell line authentication used.	Cell line authentication was performed by the University of Arizona (USA) Genetics Core based on criteria established by the International Cell Line Authentication Committee. Short tandem repeat (STR) profiling revealed that these cell lines were above the 80% match threshold.
c. Report whether the cell lines were tested for mycoplasma contamination.	Low passage working banks of cells were tested for mycoplasma using the MycoAlert detection kit according to the manufacturer's (Lonza) instructions. Mycoplasma testing and authentication are routinely performed before and after molecular engineering.
d. If any of the cell lines used are listed in the database of commonly misidentified cell lines maintained by ICLAC, provide a scientific rationale for their use.	NALM-6, OSU-CLL, K562 and HEK293T cell lines are not listed in the latest version of the database of commonly misidentified cell lines maintained by ICLAC (Version 8.0, released 1 December 2016).

Animals and human research participants

Policy information about studies involving animals; when reporting animal research, follow the ARRIVE guidelines

11. Description of research animals

Provide details on animals and/or animal-derived materials used in the study.	N/A

Policy information about studies involving human research participants

12. Description of human research participants

Describe the covariate-relevant population characteristics of the human research participants.	We did not perform covariate analyses in this secondary correlative investigation.

nature research

Corresponding author(s): Jan Joseph Melenhorst, Ph.D. and Carl H. June, M.D.

Flow Cytometry Reporting Summary

Form fields will expand as needed. Please do not leave fields blank.

Data presentation

For all flow cytometry data, confirm that:

☒ 1. The axis labels state the marker and fluorochrome used (e.g. CD4-FITC).

☒ 2. The axis scales are clearly visible. Include numbers along axes only for bottom left plot of group (a 'group' is an analysis of identical markers).

☒ 3. All plots are contour plots with outliers or pseudocolor plots.

☒ 4. A numerical value for number of cells or percentage (with statistics) is provided.

Methodological details

5. Describe the sample preparation.	Primary human PBMC or T-cells were isolated from the peripheral blood of CLL patients and healthy donors. Immunophenotyping was performed by surface staining with flow cytometry antibodies immediately following pre-incubation with Aqua Blue dead cell exclusion dye (Invitrogen). For intracellular staining, cells were fixed and permeabilized using the Foxp3 Fixation/Permeabilization Kit (eBioscience) or the Cytofix/Cytoperm Kit (BD Biosciences). The GolgiStop protein transport inhibitor containing monensin and GolgiPlug protein transport inhibitor containing brefeldin A (BD Biosciences) were used when staining for intracellular cytokine production.
6. Identify the instrument used for data collection.	Samples were acquired on a custom 17-color, 19-parameter special order LSRFortessa (BD Biosciences). Routinemeasurements of the expansion and persistence of CAR T-cells, as well as peripheral B-CLL burden were conducted with a six-parameter Accuri C6 flow cytometer (BD Biosciences).
7. Describe the software used to collect and analyze the flow cytometry data.	Data were analyzed using FlowJo software (TreeStar).
8. Describe the abundance of the relevant cell populations within post-sort fractions.	Cell frequencies/abundances are listed in the flow plot (insets).
9. Describe the gating strategy used.	Gating strategies are depicted in Extended Data Figure 2.

Tick this box to confirm that a figure exemplifying the gating strategy is provided in the Supplementary Information. ☒